Global Change Biology

Global Change Biology (2016), doi: 10.1111/gcb.13442

Do dynamic global vegetation models capture the seasonality of carbon fluxes in the Amazon basin? A data-model intercomparison

NATALIA RESTREPO-COUPE[1,2], NAOMI M. LEVINE[3,4], BRADLEY O. CHRISTOFFERSEN[2,5,6], LOREN P. ALBERT[2], JIN WU[2,7], MARCOS H. COSTA[8], DAVID GALBRAITH[9], HEWLLEY IMBUZEIRO[8], GIORDANE MARTINS[10], ALESSANDRO C. DA ARAUJO[10,11], YADVINDER S. MALHI[12], XUBIN ZENG[6], PAUL MOORCROFT[4] and SCOTT R. SALESKA[2]

[1]*Plant Functional Biology and Climate Change Cluster, University of Technology Sydney, Sydney, NSW, Australia,* [2]*Department of Ecology and Evolutionary Biology, University of Arizona, Tucson, AZ, USA,* [3]*Department of Biological Sciences, University of Southern California, Los Angeles, CA, USA,* [4]*Department of Organismic and Evolutionary Biology, Harvard University, Cambridge, MA, USA,* [5]*Earth and Environmental Sciences Division, Los Alamos National Laboratory, Los Alamos, NM, USA,* [6]*Department of Atmospheric Sciences, University of Arizona, Tucson, AZ, USA,* [7]*Biological, Environmental & Climate Sciences Department, Brookhaven National Lab, Upton, NY, USA,* [8]*Department of Agricultural Engineering, Federal University of Vicosa, Vicosa, Brazil,* [9]*School of Geography, University of Leeds, Leeds, UK,* [10]*Instituto Nacional de Pesquisas da Amazônia (INPA), Manaus, Brazil,* [11]*Embrapa Amazônia Oriental, Belem, Brazil,* [12]*Environmental Change Institute, School of Geography and the Environment, University of Oxford, Oxford, UK*

Abstract

To predict forest response to long-term climate change with high confidence requires that dynamic global vegetation models (DGVMs) be successfully tested against ecosystem response to short-term variations in environmental drivers, including regular seasonal patterns. Here, we used an integrated dataset from four forests in the Brasil flux network, spanning a range of dry-season intensities and lengths, to determine how well four state-of-the-art models (IBIS, ED2, JULES, and CLM3.5) simulated the seasonality of carbon exchanges in Amazonian tropical forests. We found that most DGVMs poorly represented the annual cycle of gross primary productivity (GPP), of photosynthetic capacity (Pc), and of other fluxes and pools. Models simulated consistent dry-season declines in GPP in the equatorial Amazon (Manaus K34, Santarem K67, and Caxiuanã CAX); a contrast to observed GPP increases. Model simulated dry-season GPP reductions were driven by an external environmental factor, 'soil water stress' and consequently by a constant or decreasing photosynthetic infrastructure (Pc), while observed dry-season GPP resulted from a combination of internal biological (leaf-flush and abscission and increased Pc) and environmental (incoming radiation) causes. Moreover, we found models generally overestimated observed seasonal net ecosystem exchange (NEE) and respiration (R_e) at equatorial locations. In contrast, a southern Amazon forest (Jarú RJA) exhibited dry-season declines in GPP and R_e consistent with most DGVMs simulations. While water limitation was represented in models and the primary driver of seasonal photosynthesis in southern Amazonia, changes in internal biophysical processes, light-harvesting adaptations (e.g., variations in leaf area index (LAI) and increasing leaf-level assimilation rate related to leaf demography), and allocation lags between leaf and wood, dominated equatorial Amazon carbon flux dynamics and were deficient or absent from current model formulations. Correctly simulating flux seasonality at tropical forests requires a greater understanding and the incorporation of internal biophysical mechanisms in future model developments.

Keywords: Amazonia, carbon dynamics, dynamic global vegetation models, ecosystem–climate interactions, eddy covariance, seasonality, tropical forests phenology

Received 10 March 2016 and accepted 18 April 2016

Introduction

Dynamic global vegetation models (DGVMs) are the most widely used and appropriate tool for predicting large-scale responses of vegetation to future climate scenarios. However, to forecast the future of Amazonia under climate change remains a challenge. The previous generation of DGVMs produced projections for Amazonia's ecosystems that diverged widely, with outcomes ranging from large-scale forest dieback to forest resilience (Betts *et al.*, 2004; Friedlingstein *et al.*, 2006; Baker *et al.*, 2008). More recent DGVM simulations showed the large-scale die-off scenario to be unlikely

Correspondence: Natalia Restrepo-Coupe, tel. +1 647 328 1494, fax +1 647 328 1494, e-mail: nataliacoupe@gmail.com

(Cox *et al.*, 2013), given (i) an improved model understanding of forest response to the negative effects of temperature previously overestimated and now constrained (Cox *et al.*, 2013), and (ii) current models being forced with updated climate projections (temperature and precipitation) bounded by observations that no longer demonstrate drastic climate changes in response to rising CO_2 in the tropics (Cox *et al.*, 2013; Huntingford *et al.*, 2013). Yet tropical forest response to climate change remains uncertain as models produce varying outcomes (Shao *et al.*, 2013) even without die-off. Some cutting-edge DGVMs projected forest degradation due to future deforestation and increasing temperature, with catastrophic consequences for the global climate based on climate–carbon cycle feedbacks (Wang *et al.*, 2013, 2014; Friend *et al.*, 2014), while other DGVMs foresaw strong carbon sinks in these forests due to CO_2 fertilization of photosynthesis (Rammig *et al.*, 2010; Ahlström *et al.*, 2012; Huntingford *et al.*, 2013; Friend *et al.*, 2014). Although the effects of temperature, water limitation, and CO_2 fertilization mechanisms remain uncertain, all DGVMs continue to agree that Amazonian forests play an important role in regulating the global carbon and water cycle (Eltahir & Bras, 1994; Werth & Avissar, 2002; Wang *et al.*, 2013, 2014; Ahlström *et al.*, 2015).

Key to reducing uncertainty in DGVMs is their systematic evaluation against observational datasets. This exercise enables the identification of model deficiencies through comparison with observed patterns in ecosystem processes, as well as the mechanisms underpinning such processes (Baker *et al.*, 2008; Christoffersen *et al.*, 2014). Recent model-data evaluations in tropical forests have focused on the cascade of ecosystem responses to long-term droughts (Powell *et al.*, 2013) and the definition of spatial patterns in productivity and biomass (Delbart *et al.*, 2010; Castanho *et al.*, 2013). However, one important context for model assessment in tropical forests is in the seasonality of ecosystem water and carbon exchange, as observational datasets reveal axes of variation in productivity, biomass and/or forest function across space (da Rocha *et al.*, 2009; Restrepo-Coupe *et al.*, 2013), and/or through time (Saleska *et al.*, 2003; von Randow *et al.*, 2004; Hutyra *et al.*, 2007; Brando *et al.*, 2010). The most consistent temporal variation in tropical forests is the seasonality of water, energy, and carbon exchange, as all tropical ecosystems are seasonal in terms of insolation and a majority experience recurrent changes in precipitation, temperature, and/or day length. Evaluation with respect to seasonality has typically focused on evapotranspiration (ET) (Shuttleworth, 1988; Werth & Avissar, 2002; Christoffersen *et al.*, 2014) and on net carbon exchange (NEE) (Baker *et al.*, 2008; von Randow *et al.*, 2013; Melton *et al.*, 2015). Where models compensated misrepresentations of gross primary productivity (GPP) in the NEE balance, by improving or adjusting the efflux term represented by heterotrophic (Melton *et al.*, 2015) or ecosystem respiration (Baker *et al.*, 2008) to available moisture among other strategies. Only recently have the seasonal dynamics of GPP drawn the attention of different groups (De Weirdt *et al.*, 2012; Kim *et al.*, 2012) and where Kim *et al.* (2012) demonstrated that a consequence of its incorrect derivation was to overestimate the vulnerability of tropical forests to climate extremes. Therefore, identifying discrepancies in observed vs. modeled seasonality in carbon flux even when seasonal amplitudes are not large, as can be the case for evergreen tropical forests (see LP Albert, N Restrepo-Coupe, MN Smith *et al.* (submitted) for cryptic phenology), can lead to important model developments with significant consequences to obtain better projections of the fate of tropical ecosystems under present and future climate scenarios.

Analysis of eddy covariance datasets has shown that in non-water-limited forests of Amazonia, the observed seasonality of GPP was not exclusively controlled by seasonal variations in light quantity (as has been demonstrated for ET) or water availability. Instead, GPP was driven by a combination of incoming radiation and phenological rhythms influencing leaf quantity (measured as leaf area index; LAI) and quality (leaf-level photosynthetic capacity as a function of time since leaf-flush) (Restrepo-Coupe *et al.*, 2013; Wu *et al.*, 2016). The lack of a direct correlation between GPP and climate suggests that ecosystem models that are missing sufficient detail of canopy leaf phenology will likely not capture seasonal productivity patterns. Accordingly, recent studies showed model simulations (ED2 and ORCHIDEE) to be deficient in terms of predicted seasonality in GPP and litter-fall, if missing leaf demography and turnover as in Kim *et al.* (2012) and in De Weirdt *et al.* (2012), respectively. Between the two studies, only two sites (eastern 'K67' and northeastern ('CAX') were represented, both of which experience very similar precipitation and light regimes. This further highlights the need for expanded evaluation of modeled seasonality of GPP across a range of sites spanning a broader range of climates and phenologies.

If the improved representation of the dynamics of leaves and other carbon pools translates into more accurate simulations of seasonal GPP and/or the long-term carbon budget (De Weirdt *et al.*, 2012; Kim *et al.*, 2012; Melton *et al.*, 2015), then comparisons between observations and model-derived seasonality of carbon allocation could provide insight into the mechanistic response of vegetation to climate and strategies to incorporate them into DGVMs. For example, critically evaluating the seasonality of net primary production of

leaves (NPP_{leaf}) and wood (NPP_{wood}) in tandem with photosynthesis will inform deficiencies in model allocation schemes and carbon pool residence times. Model net primary production (NPP) typically arises from the allocation of photosynthate to main organs, either as a constant fraction of GPP (Kucharik *et al.*, 2006), or according to fixed allometric rules (Sitch *et al.*, 2003). However, such a view of supply-limited growth has come into question recently (Würth *et al.*, 2005; Fatichi *et al.*, 2014). Thus, as water, temperature, and nutrients can all impact cell expansion, there may be a temporary imbalance between carbon used for tissue growth and maintenance respiration vs. carbon supplied by assimilation (photosynthesis) (Fatichi *et al.*, 2014). Patterns in seasonality of GPP, $NPP_{leaf,}$ and NPP_{wood}, therefore, potentially reveal the degree of coupling (or lack thereof) of these two carbon sinks (NPP_{wood} and NPP_{leaf}) with photosynthetic activity (GPP). Indeed, Doughty *et al.* (2014) used bottom-up estimates of the ecosystem carbon budget at a forest in southwest Amazonia and showed that components of NPP varied independently of photosynthetic supply, which they interpreted in terms of theories of optimal allocation patterns. While an alternative interpretation of such patterns could simply refer to biophysical limitations on growth, which vary seasonally (Fatichi *et al.*, 2014), both studies suggest that modeling allocation as a function of GPP will likely fail to capture observed seasonality. Ground-based bottom-up estimates of primary productivity at a temporal resolution greater than a year (i.e., seasonal) are difficult if not impossible, principally because there is no accepted method for estimating whole-tree nonstructural carbon (NSC) and its variation with seasons (Würth *et al.*, 2005; Richardson *et al.*, 2015). We propose coupling colocated top-down eddy flux estimates of GPP with bottom-up NPP estimates (NPP_{wood}, $NPP_{leaf,}$ and $NPP_{litter\text{-}fall}$) to circumvent this problem and to obtain a better informed view of the mechanisms (e.g., allocation schemes) models may incorporate or test against, to improve seasonal simulations of carbon fluxes and pools.

The focus of this study was to evaluate, for the first time, modeled seasonal cycles of different carbon pools and fluxes, including leaf area index (LAI), GPP, leaf-fall, leaf-flush, and wood production, with high-resolution eddy flux estimates of GPP and ground-based surveys. We centered our study on a comparison between forests located in the equatorial Amazon (radiation- and phenology-driven) to a southern forest (driven by water availability) and explored the different model strategies to incorporate and simulate physical and ecological drivers. Here, we assessed four state-of-the-art DGVMs in active development for use in coupled climate–carbon cycle simulations in terms of whether they could simultaneously determine patterns of growth and photosynthesis, thereby getting the 'right answer for the right reason'. We conclude by proposing several approaches for improving model formulations and highlight the need for model-informed field campaigns and future experimental designs.

Materials and methods

Site descriptions

We analyzed data from the Brazil flux network for four tropical forests represented by the southern site of Reserva Jarú (RJA), and three central Amazonia forests (~3°S) from west to east: the Reserva Cuieiras near Manaus (K34), the Tapajós National forest, near Santarém (K67), and the Caxiuanã National forest near Belém (CAX) (Fig. 1). For detailed site information see previous works by Restrepo-Coupe *et al.* (2013), and de Goncalves *et al.* (2009); de Gonçalves *et al.* (2013) and individual site publications (Araújo *et al.*, 2002; Carswell *et al.*, 2002; Malhi *et al.*, 2002; Saleska *et al.*, 2003; Kruijt *et al.*, 2004; von Randow *et al.*, 2004; Hutyra *et al.*, 2007; da Costa *et al.*, 2010; Baker *et al.*, 2013).

All study sites had mean annual precipitation (MAP) above 2000 mm yr^{-1} (Fig. S1 and Table 1), based on the 1998–2014 satellite-derived precipitation from the Tropical Rainfall Measuring Mission (TRMM 3B43-v7 at a resolution of 0.25 deg) (Huffman *et al.*, 2007; NASA, 2014). See Fig. S10 for a comparison between observations and TRMM data. CAX and K34 had MAP over 2500 mm yr^{-1}, 2572, and 2673 mm yr^{-1}, respectively (Fig. S11). By contrast, at the southern forest of RJA and at the equatorial forest of K67 MAP was ~2030 mm yr^{-1}. We defined the dry season as those periods where precipitation was less than ~100 mm $month^{-1}$ (Sombroek, 2001; da Rocha *et al.*, 2004; Restrepo-Coupe *et al.*, 2013). The 100 mm $month^{-1}$ threshold corresponds to ~90% of the observed annual maximum 16-day ET averaged across years (115 ± 12 mm $month^{-1}$) and close to the mean seasonal ET (92 ± 1.5 mm $month^{-1}$) at the four tropical forests here reported (Restrepo-Coupe *et al.*, 2013). Based on the 16-year TRMM series, RJA had a 5-month dry-season length (DSL) comparable to two of the central Amazon sites of CAX and K67 (4–5 months); however, longer than at the equatorial Amazon K34 forest (1–2-months). RJA and K67 showed similar mean dry-season precipitation (46 mm $month^{-1}$ at RJA and 64 mm $month^{-1}$ at K67). However, the annual minimum averaged across the years 1998–2014 (*MiAP*) at RJA was 15 mm $month^{-1}$ compared to a more benign dry season minimum of 36 mm $month^{-1}$ at K67 (Figs. 1 and S11, and Table 1). Despite being located at a latitude further from the equator (10°S), incoming photosynthetic active radiation (PAR) at the southern forest of Jarú was less seasonal (lower amplitude) if compared to the central Amazon forests (latitude ~3°S) (Fig. 2). At RJA, the period of peak top of the atmosphere radiation (TOA) was synchronous with the wet season – when we expected higher reflectance by clouds to decrease the surface available PAR (Fig. 2). All equatorial sites sat on highly weathered deep clay soils (≥10 m), whereas RJA sat on a lower

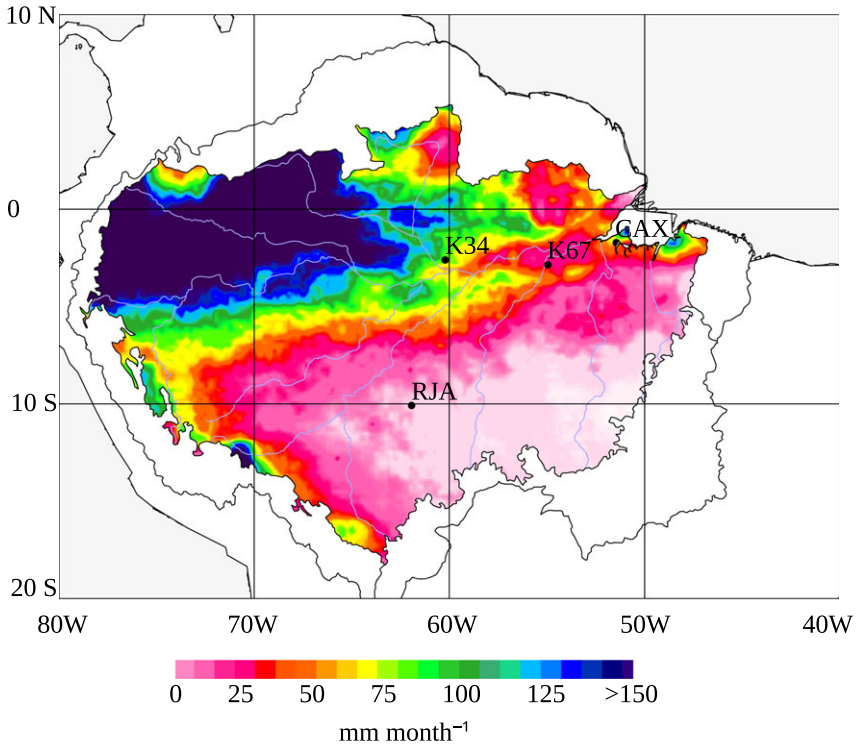

Fig. 1 Locations of eddy covariance tower study sites at the Amazon Basin *sensu stricto* (Eva & Huber, 2005 eds). Minimum monthly precipitation (mm month^{-1}) from the Tropical Rainfall Measuring Mission (TRMM) (NASA, 2014) based on an annual composite for the years 1998 to 2014.

Table 1 Precipitation at Amazon basin study sites. Based on the tropical rainfall measuring mission (TRMM) (NASA, 2014) for the years 1998 to 2014

Site	Latitude	Longitude	Mean annual precipitation MAP (mm yr^{-1})	Dry-season precipitation DSP (mm month^{-1})	Dry-season length DSL (months)	Annual minimum average precipitation *MiAP* (mm month^{-1})
K34	−2.61	−60.21	2672.6	99.7	1*	99.7
CAX	−1.72	−51.53	2571.8	78.8	4	59.5
K67	−2.86	−54.96	2037.8	63.7	4*	36.2
RJA	−10.08	−61.93	2019.3	46.2	5	14.6

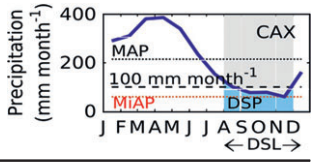

*1+ month DSL if defined as rain<103 mm month^{-1}. TRMM 1998–2014.

water storage capacity loamy sandy soil and a more shallow and variable profile, with depth to bedrock as shallow as 2–3 m (Hodnett *et al.*, 1996; Christoffersen *et al.*, 2014).

Eddy covariance methods

At the above-mentioned forests, climate, carbon, energy, water, and momentum fluxes were measured by the eddy covariance (EC) method. Meteorological measurements included vapor pressure (VPD), air temperature (T_{air}), PAR, and incoming and outgoing short- and long-wave radiations, among others. We estimated the cloudiness index (CI), a proxy for light quality, based on the observed PAR and the theoretical PAR (PAR_{theo}). The PAR_{theo} was computed following Goudriaan (1986) top of the atmosphere radiation and scaled to fit monthly maximum observed PAR for the hour across years. The CI ranges from 0 to 1, from diffuse to direct irradiance dominating incoming PAR value, respectively:

$$CI = 1 - \frac{PAR_{obs}}{PAR_{theo}}. \quad (1)$$

Starting with half-hourly CO_2 flux data provided from each site's operator, we calculated net ecosystem exchange (NEE in μmol CO_2 m^{-2} s^{-1}), with fluxes to the atmosphere defined as positive. NEE was then filtered for low turbulence periods (u^*_{thresh}). For a detailed description of instrumentation, data

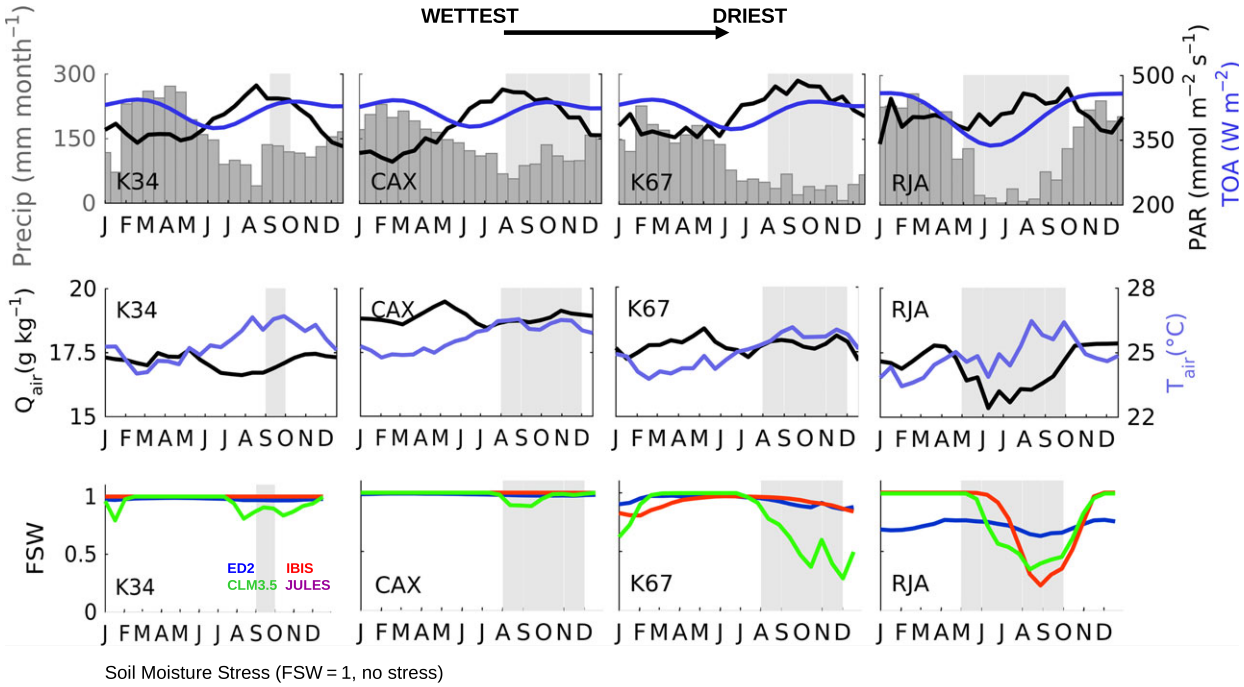

Fig. 2 From top to bottom annual cycle of daily average observed climatic variables: incoming photosynthetic active radiation (PAR; μmol m^{-2} s^{-1}, black line right *y*-axis) and precipitation (*Precip*; mm $month^{-1}$, dark gray bars left *y*-axis), top of the atmosphere incoming radiation (TOA; W m^{-2}, blue line right *y*-axis) (not a driver). From left to right study sites (from wettest to driest) near Manaus (K34), Caxiuanã (CAX), Santarém (K67), and Reserva Jarú southern (RJA) forests. Gray-shaded area is dry season as defined using satellite-derived measures of precipitation (TRMM: 1998–2014). Second-row LSM drivers: near-surface specific humidity (Q_{air}; g kg^{-1}, black line left *y*-axis) and temperature (T_{air}; °C, blue line right *y*-axis). Lower panel depicts model ecosystem-scale of model soil moisture 'stress' (FSW, where 1 = no stress). Simulations from ED2 (blue), IBIS (red), CLM3.5 (green), and JULES (purple).

processing, applied corrections, quality control procedures, and the effect of u^*_{thresh} on NEE calculations refer to Restrepo-Coupe *et al.* (2013). Gross ecosystem exchange (GEE) was derived from tower measurements of daytime NEE by subtracting estimates of ecosystem respiration (R_e), which we derived from the nighttime NEE. We assumed daytime R_e was the same as nighttime R_e, as we did not observe a statistically significant within-month correlation between nighttime hourly NEE and nighttime T_{air} (Restrepo-Coupe *et al.*, 2013). GEE is a negative value (GEE = NEE - R_e) as generally NEE is negative in the daytime, and R_e is positive (meteorological convention). We expressed ecosystem-scale photosynthesis or gross ecosystem productivity (GEP), as negative GEE and assumed negligible re-assimilation of metabolic respiration CO_2 within the leaf and insignificant CO_2 recirculation below the EC system (Stoy *et al.*, 2006). For comparison with model output, we used GEP interchangeably with gross primary productivity (GPP).

We defined ecosystem photosynthetic capacity (Pc, gC m^{-2} day^{-1}) as the 16-day GPP averaged over a fixed narrow range of reference climatic conditions following some of the modifications introduced by Wu *et al.* (2016) (e.g., including CI and T_{air} on its calculations) to Pc used in Restrepo-Coupe *et al.* (2013). For our analysis, Pc was estimated as the rate of carbon fixation under reference conditions defined by fixed narrow bins in: site specific daytime annual mean PAR ± 150 μmol m^{-2} s^{-1}, VPD, T_{air}, and CI ± 1.5 standard deviation from their respective means (see Table S1). Thus, Pc, by definition, removed the effect of day-to-day changes in available light, diffuse/direct radiation, photoperiod, temperature, and atmospheric demand from photosynthesis. The Pc has been shown to be a robust representation of the emergent photosynthetic infrastructure of the whole forest canopy (Wu *et al.*, 2016).

We looked at evapotranspiration (ET, mm day^{-1}) calculated as the latent heat flux (LE, W m^{-2}) measured at the tower multiplied by the latent heat of vaporization (λ, kJ kg^{-1}). We developed a Type II linear model between surface incident short-wave radiation (SW_{down}, W m^{-2}) and the dependent variable, ET.

From the standard suite of climatic variables available for periods between 1999 and 2006 measured at each EC tower, meteorological drivers for the models were generated. According to Rosolem *et al.* (2008), the selected periods represent the mean climatological condition and exclude anomalous climatic events (e.g., 2010 El Niño-Southern Oscillation (ENSO) or 2005 drought as experienced at the southern Amazon). Variables included the following: SW_{down}; air temperature (T_{air}, °K); near-surface specific humidity (Q_{air}, g kg^{-1}); rainfall (*Precip*, mm $month^{-1}$); magnitude of near-surface wind (WS, m s^{-1}); surface atmospheric pressure (Pa, hPa); surface incident long-wave radiation (LW_{down}, W m^{-2}); and CO_2 concentration ($CO_{2\ air}$) was fixed at 375 ppm (de Goncalves

et al., 2009) (Fig. 2). Drivers were created for consecutive years where gaps were no greater than two months. All time series were subject to quality control (e.g., removal of outliers) and then filled using other tower measurements (e.g., from a temperature profile), nearby sites and/or the variable's mean monthly diurnal cycle (Stockli, 2007). We analyzed data for 2000–2005 for K34, 2002–2004 for K67, 2000–2002 for RJA, and 1999–2003 for CAX. We restricted flux and meteorological observations and the calculation of seasonality to the abovementioned dates in order to match model drivers and output.

Hourly fluxes (GPP, NEE, $R_{e,}$ and ET) and meteorology were aggregated to 16-day time periods, assuming that at least 4 days were available with at least 21 h of observations each. Gaps were not filled further and mean annual cycles were then calculated.

Field measurements

Although field measurements can be translated into carbon storage values (e.g., wood carbon pool from DBH inventories via allometric equations), we focused on departures from a base level because they reflect the seasonality of allocation. The following vegetation infrastructure descriptors and carbon pools were included in the analysis:

Leaf Area Index (LAI): model output was compared to LAI observations for Caxiuanã, CAX as reported by Metcalfe *et al.* (2007), and for Santarem, K67 as by Brando *et al.* (2010). LAI was normalized from 0 to 1 ($LAI_{normalized}$) for purposes of presentation. Thus, in order to emphasize and visualize any seasonal changes in LAI, independent of the observed or modeled absolute value, we used Eqn (2), where at time i, LAI_i was adjusted by LAI_{min} and LAI_{max} that corresponded to the minimum and maximum seasonal LAI, respectively:

$$LAI_{normalized(i)} = \frac{LAI_i - LAI_{min}}{LAI_{max} - LAI_{min}}. \quad (2)$$

Leaf litter-fall or net primary productivity allocated to litterfall ($NPP_{litter\text{-}fall}$, gC m^{-2} day^{-1}): values corresponded to monthly litter-bed measurements at Manaus, K34 (here presented for the first time), and to those reported by Rice *et al.* (2004) for K67 and by Fisher *et al.* (2007) for CAX.

Modeled NPP_{leaf} followed a basic leaf balance model proposed by Restrepo-Coupe *et al.* (2013). Assuming the change in ecosystem Pc (dPc/dt) to be driven by (i) the loss or gain of leaves, $NPP_{litter\text{-}fall,}$ and NPP_{leaf}, respectively (quantity), and (ii) the changes in leaf-level carbon assimilation at saturating light (SLA x A_{max}) related to age (quality), and therefore, solving for leaf production we obtained:

$$NPP_{leaf} = NPP_{litter-fall} + \frac{1}{A_{max} \times SLA} \times \frac{dPc}{dt} \quad (3)$$

where specific leaf area (SLA) values were set to 0.0140 for K67 and CAX (Domingues *et al.*, 2005), 0.0164 m^2 per gC for K34 (Carswell *et al.*, 2002). The A_{max} was reduced to reach 40% of the mean value at the time when leaf-fall reached its maximum (2-month linear gradient). Maximum A_{max} was set to 8.66 gC m^{-2} day^{-1} at K67 (Domingues *et al.*, 2005), and to 7.36 gC m^{-2} day^{-1} at K34 (Carswell *et al.*, 2000) and CAX.

Wood net primary productivity (NPP_{wood}) was based on stem wood increment measurements (diameter at breast height, DBH) as reported by Rice *et al.* (2004) at K67, Chambers *et al.* (2013) at K34, and da Costa *et al.* (2010) at CAX and on allometric equations as proposed by in Chambers *et al.* (2001). No data were available for RJA.

Dynamic global vegetation models (DGVMs)

We presented output from four state-of-the-art dynamic global vegetation models. All DGVMs were process based (e.g., photosynthesis, respiration, and evapotranspiration) and able to simulate the fluxes of carbon, water, and energy between the atmosphere and the land surface (see Tables S2 and S3). The model simulations were run as part of the Interactions between Climate, Forests, and Land Use in the Amazon Basin: Modeling and Mitigating Large Scale Savannization project (Powell *et al.*, 2013;).

To standardize all physical parameters within the models so as to focus on agreements and discrepancies among the different biomass schemes, all four DGVMs used the same soil hydrology properties (including free drainage conditions), and soil physical parameters and depths. The spin-up protocol consisted of running each model from near-bare-ground until variations in soil moisture, slow soil carbon, and aboveground biomass were <0.5% (defined as average change for the last cycle of meteorological forcing as compared to the previous cycle). Atmospheric CO_2 concentrations were set to pre-industrial values (278 ppm) and later increased to present day starting in 1715 (considered as the first year after stabilization). Radiation was split between direct and diffuse following Goudriaan (1977). We summarized each DGVM's carbon flux, and vegetation dynamics formulation in Tables S2 and S3, and briefly describe the four models in this section:

Ecosystem Demography model version 2 (ED2): ED2 is an individual-based terrestrial biosphere model providing a physically and biologically consistent framework suitable for both short-term (hourly to interannual) and long-term (interannual to multicentury) studies of carbon, water, energy fluxes, and associated dynamics of terrestrial ecosystem composition structure and function. It uses a system of size- and age-structured partial differential equations (PDEs) to describe the behavior of a vertically stratified, spatially distributed, ensemble of individual plants within each climatological grid cell that undergo spatially localized height-structured competition for light and water (Moorcroft *et al.*, 2001; Medvigy *et al.*, 2009). ED2 uses four plant functional types (PFT) for the tropics (early-, mid- and late-successional tropical forest trees, and C_4 grasses). The model ran on a 10-min time step. The physiological dynamics of each individual component (photosynthesis, transpiration, carbon allocation, biomass growth, mortality, etc.) were tracked independently. The structure and composition of the ecosystem within each grid cell were not prescribed, but rather emerged from the demographic dynamics (growth, mortality, recruitment) of the plants within the canopy. ED2 tracked three different soil carbon pools for each layer (fast, slow, and structural), and the water extraction depth of plants varied according to their size and PFT identity.

The model did not include hydraulic redistribution. The ED2's PFT's photosynthetic parameters (maximum photosynthetic capacity and dark respiration) were adjusted using site-level measurements of GPP, net ecosystem productivity (NEP), and aboveground biomass (AGB) from K34 flux tower site as part of a related study (Levine *et al*., 2016).

Integrated Biosphere Simulator (IBIS): The tropical rainforest vegetation in IBIS is a composite of four plant functional types, 'tropical evergreen tree', 'tropical deciduous tree', 'C3 grass', and 'C4 grass', that compete for water and light. The model simulated hourly carbon fluxes using the Ball-Berry–Farquhar equations (Farquhar *et al*., 1980). LAI was calculated annually using a fixed coefficient for allocation to the leaves (0.3) and fixed residence times (12 months), although a water stress function could seasonally drop leaves in the case of the tropical deciduous trees. Biomass was integrated over the year using a similar procedure (Foley *et al*., 1996). The IBIS version used here simulated six soil layers with a total depth of 8 m; water extraction by the roots varied by layer and was controlled by a root distribution parameter. IBIS required 76 parameters to be specified, of those 14 were related to soil, 12 were specific to each of the nine PFTs, and 50 were related to morphological and biophysical characteristics of vegetation.

Community Land Model-Dynamic Global Vegetation Model version 3.5 (CLM3.5): The predecessor to the current CLM4-CNDV model (Gotangco Castillo *et al*., 2012), which is the land component of the Community Earth System Model (CESM). CLM3.5 runs were set using a prognostic phenology, which incorporated recent improvements to its canopy interception scheme, new parameterizations for canopy integration, a TOPMODEL-based model for runoff, canopy interception, soil water availability, soil evaporation, water table depth determination by the inclusion of a groundwater model, and nitrogen constraints on plant productivity (without explicit nitrogen cycling) (Oleson *et al*., 2008). The model treated the canopy as a weighted average (by their respective *LAI*s) of sunlit and shaded leaves. The leaf phenology subroutine of this model for tropical forests applied only to the Broadleaf Deciduous Tree (BDT) PFT fraction ('raingreen' PFT), but all CLM3.5 simulations reported here were >95% tropical Broadleaf Evergreen Tree (BET) fractional PFT cover. The allocation scheme for this model dictated that leaf turnover for the tropical BET (at a rate of 0.5 per year) be replaced instantaneously with new leaf production to maintain fixed allometric relationships (Sitch *et al*., 2003); therefore, seasonality of LAI was not possible for these simulations.

Joint UK Land Environment Simulator (JULES): The UK community land surface model was described in Best *et al.* (2011) and Clark *et al.* (2011). Simulations for this study were conducted using JULES v2.1, which did not simulate drought deciduous vegetation. The model represents five PFTs globally, of which the 'evergreen broad-leaved tree' PFT dominates over Amazonia. Gross leaf-level photosynthesis was based on Collatz *et al.* (1991, 1992) and was calculated as the smoothed minimum of three potentially limiting rates: a rubisco-limited, a light-limited, and the rate of transport of photosynthetic assimilates. Plant respiration was simulated as a function of tissue temperature and nitrogen concentrations. Soil moisture stress effects were incorporated by scaling potential net photosynthesis rate with a simple β factor (Cox *et al*., 1999; Powell *et al*., 2013). Leaf-level photosynthesis was coupled with stomatal conductance using the formulation by Jacobs (1994). Photosynthesis was scaled from leaf to canopy using a 10-layer canopy model, which adopts the two-stream approximation of radiation interception from Sellers (1985). NEP was partitioned into a fraction used for growth and a fraction used for the 'spreading' of vegetation. Carbon for growth was allocated to three vegetation pools (wood, roots, leaves) following specific allometric relationships between pools (Clark *et al*., 2011).

DGVMs output followed the LBA-Data Model Intercomparison Project (LBA-DMIP) protocol (de de Goncalves *et al*., 2009); however, they included some additional variables related to water limitation (e.g., soil water availability factor or soil water 'stress'), land use change (e.g., additional carbon pools), and disturbance (e.g., mortality) (Powell *et al*., 2013). Here, we present soil water 'stress' (FSW) values, calculated following Ju *et al.* (2006). By definition FSW ranges from 0 to 1, and it is a measure of the water available to roots, where FSW = 1, is no stress.

Models were compared to observations based on the timing and amplitude metrics of their annual cycle. Statistical descriptors as correlation coefficient (R), root-mean-square difference, and the ratio of models to observations standard deviations were calculated for the 16-day time series for multiple years and summarized using the Taylor diagrams (Taylor, 2001).

Results

Gross primary productivity (GPP) and ecosystem photosynthetic capacity (Pc)

The observed annual cycle of ecosystem-scale GPP showed two divergent patterns: (i) increasing levels of photosynthetic activity (GPP) as the dry season progresses in the equatorial Amazon (K34, K67, and CAX) where *MiAP* was 103, 60, and 37 mm month^{-1}, respectively, and maximum radiation was synchronous with low precipitation; and (ii) declining productivity as the dry season advanced in the southern forest (RJA) where radiation was somewhat aseasonal and *MiAP* was less than half its central Amazon counterparts (14 mm month^{-1}) (Fig. 3). By contrast, at all sites, model simulations showed peak GPP seasonality at the end of wet season with declining GPP during the dry season (Fig. 3). The reduced dry-season GPP observed at the southern Amazon forest of Jarú (RJA) was consistent with increasing degrees of water limitation. At the sites in the equatorial Amazon (K34, K67, and CAX), modeled soil water 'stress' (FSW; Fig. 2) (where FSW = 1, no stress) acted to reduce model GPP during the dry season, even as observed Pc increased following higher levels of incoming solar radiation (PAR; Fig. 2 and Pc; Fig. 4). Similar to GPP, models tended to achieve good

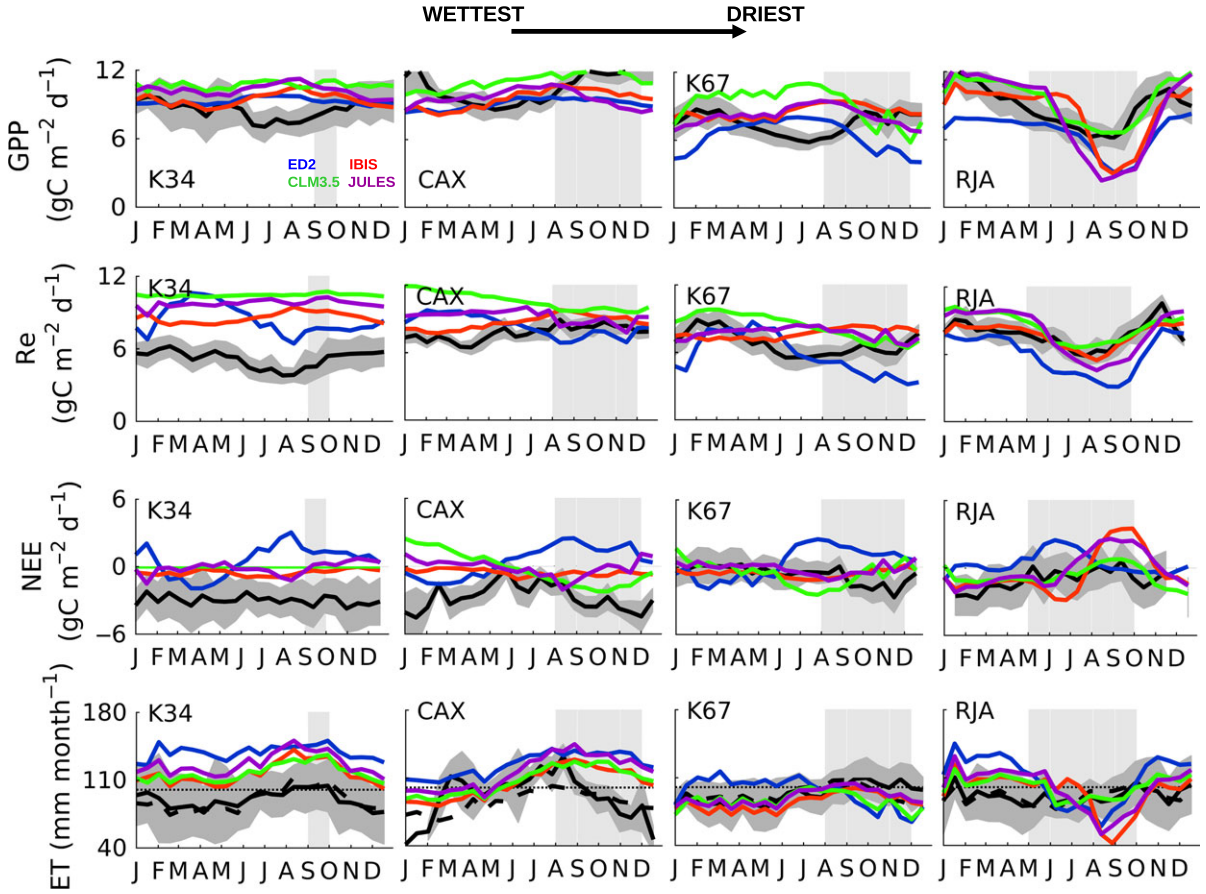

Fig. 3 Annual cycle of daily average ecosystem-scale photosynthesis (GPP; gC m^{-2} day^{-1}), ecosystem respiration (R_e; gC m^{-2} day^{-1}), net ecosystem exchange (NEE; gC m^{-2} day^{-1}), and evapotranspiration (ET; mm $month^{-1}$). From left to right study sites (from wettest to driest) near Manaus (K34), Caxiuanã (CAX), Santarém (K67), and Reserva Jarú southern (RJA) forests. Observed (black + dark gray uncertainty) and simulated by models (colors). Dashed black line at ET panels corresponds to a linear model where the independent variable is incoming radiation (SW_{down}). Gray-shaded area is dry season as defined using satellite-derived measures of precipitation (TRMM: 1998–2014). Simulations from ED2 (blue), IBIS (red), CLM3.5 (green), and JULES (purple).

Pc representation at RJA (Fig. S7). However, simulated Pc at the equatorial Amazon forest sites remained unchanged (IBIS and JULES) or decreasing gradually from the middle of the wet season to the end of the dry period at K67 (ED2 and CLM3.5) (Fig. 4).

FSW reached an all-site minimum at RJA by the end of the dry season (Fig. 2) and corresponded with a decrease in model ET not seen on the EC measurements (Fig. 3). With the exception of CAX, seasonal observations of ET at all of the sites showed very little seasonality and remained close to 92 mm $month^{-1}$ (3 mm day^{-1}). In general, DGVMs were able to capture the seasonality of ET; however, they overestimated the dry-period reduction in water exchange at RJA and in the case of K34 and CAX overestimated ET absolute values (Fig. S9). By contrast, a very simple linear regression driven by SW_{down} was able to represent ~83% of the seasonality of ET (Fig. 3).

Carbon allocation

We explored different DGVMs approaches to simulate the phenology of carbon allocation, in particular measures of plant metabolism (ecosystem photosynthetic capacity, Pc as proxy), standing biomass (wood increment, leaf production, and the balance of gain and loss of leaves), and additions to soil organic matter (leaf-fall), in an attempt understand the model-data discrepancies on the estimates of GPP, R_e, and NEE (Figs S7 and S8).

Our results indicated that none of the models were able to capture or replicate the observed dry-season LAI changes at the equatorial Amazon forests EC locations (Fig. 4). In addition, with the exception of ED2, the annual mean LAI values were unrealistically high (Baldocchi *et al.*, 1988; Gower *et al.*, 1999; Asner *et al.*, 2003; Sakaguchi *et al.*, 2011). In contrast, to some model

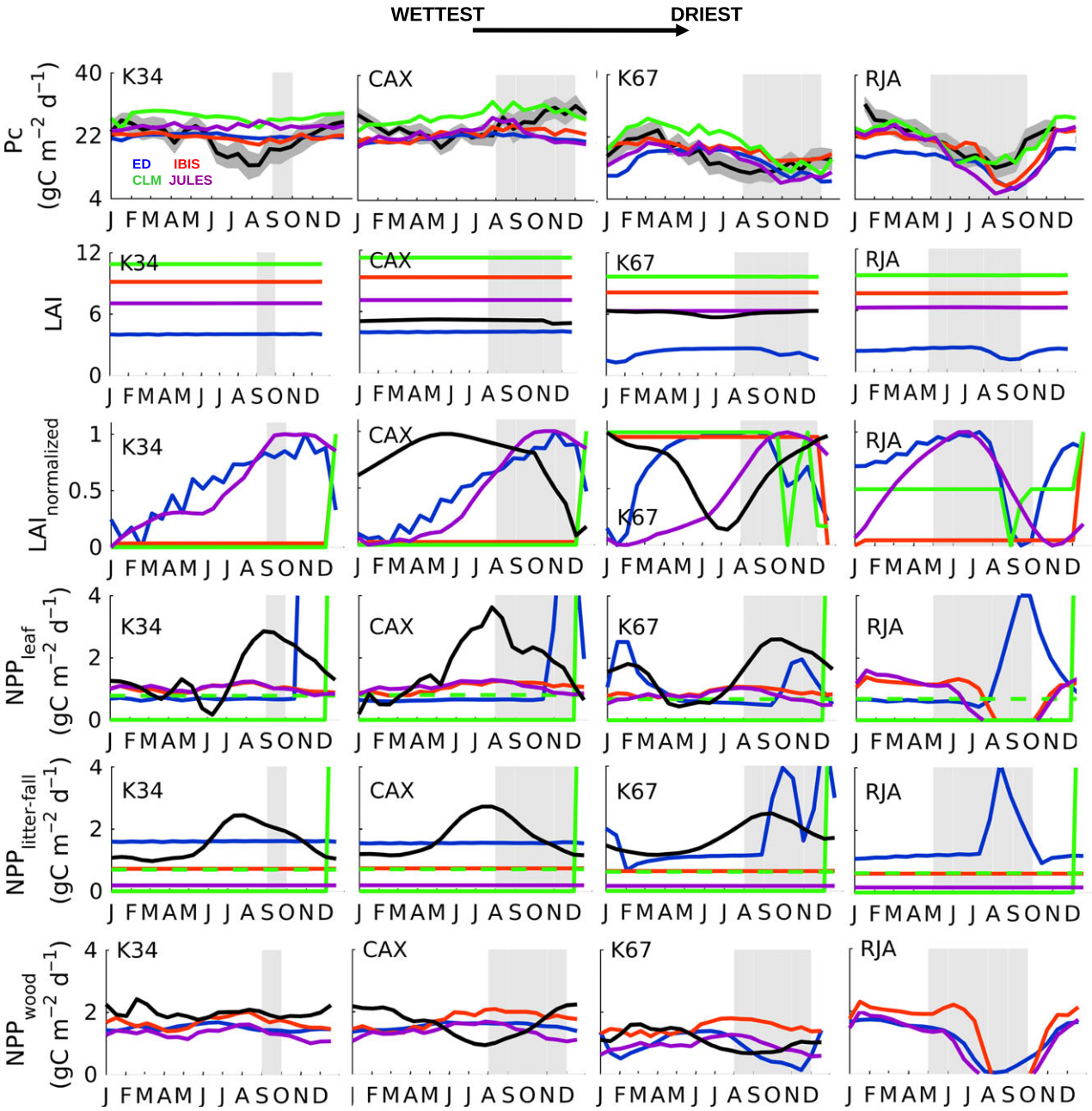

Fig. 4 From top to bottom annual cycle of daily average ecosystem photosynthetic capacity (Pc; gC m^{-2} day^{-1}), leaf area index (LAI; m^2 m^{-2}), normalized LAI (its value constrained between 0 and 1 in order to better track its changes), net primary productivity (NPP; m^{-2} day^{-1}) allocated to leaves leaf-flush (NPP_{leaf}; m^{-2} day^{-1}), NPP allocated to litter-fall ($NPP_{litter\text{-}fall}$; gC m^{-2} day^{-1}). Lower row, NPP allocated to wood (NPP_{wood}; gC m^{-2} day^{-1}). Gray-shaded area is dry season as defined using satellite-derived measures of precipitation (TRMM: 1998–2014). From left to right study sites (from wettest to driest) near Manaus (K34), Caxiuanã (CAX), Santarém (K67), and Reserva Jarú southern (RJA) forests. Observed (black) vs. simulated by models (colors). Simulations from ED2 (blue), IBIS (red), CLM3.5 (green), and JULES (purple). Dashed green lines (CLM3.5) at $NPP_{litter\text{-}fall}$ and NPP_{leaf}, indicate average values for comparison purposes (models allocated at the end of the year as indicated by continuous line).

phenology schemes that assumed LAI and T_{air} to be positively correlated, we observed nonstatistically significant positive and negative regressions slopes at CAX and K67, respectively ($R^2 < 0.1$; P-value >0.1) (Fig. S6).

In the field, leaf litter-fall plays an important role in determining the seasonality of LAI, Pc (as per Eqn 3), heterotrophic respiration, and soil carbon pools. Consistent with leaf-fall studies showing highly seasonal

cycles in $NPP_{litter\text{-}fall}$ (Chave *et al*., 2010), observations at these sites showed a highly seasonal leaf abscission cycle with maximum leaf mortality at the beginning of the dry season at CAX and in the middle of the dry period at K67 (Fig. 4). At equatorial sites, peak litter-fall corresponded to a maximum in SW_{down}, where we observed a statistically significant linear regression between SW_{down} and $NPP_{litter\text{-}fall}$ with a coefficient of determination, R^2 equal to 0.34 at K34, 0.21 at K67, and 0.6 at CAX ($P < 0.01$) (Fig. S2). With the exception of ED2, which included a drought deciduous phenology and consequentially seasonal variations in leaf abscission, seasonality in $NPP_{litter\text{-}fall}$ was not resolved in most DGVMs (Fig. 4).

Estimates of leaf production (increase in the amount of young-high photosynthetic capacity leaves) from the observations at K67 forest showed peak NPP_{leaf} in the dry season in contrast to most simulations. In general, NPP_{leaf} was as follows: (i) constant in most models; (ii) allocated at the end of the year, similar to $NPP_{litter\text{-}fall}$; or (iii) declining, in particular during the strong K67 dry season (Fig. 4). Even if counterintuitive, at some of the equatorial Amazon sites key leaf-demography processes (e.g., leaf-fall and leaf-flush) and/or LAI, increased in tandem during the dry season.

In contrast to NPP_{leaf}, NPP allocation to wood growth was aseasonal at K34; however, at K67 NPP_{wood} peaked during the wet season, displaying opposite seasonality and being out-of-phase with NPP_{leaf}. This pattern seemed to be different at CAX, where maximum NPP_{leaf} occurred at the beginning of the dry season, ahead of NPP_{wood} which steadily increased as the dry season progressed and was maintained at high levels for the first half of the wet season. At this site, precipitation was significantly seasonal (wet season was the rainiest of all equatorial sites) and the amplitude of the seasonal cycle of SW_{down} was the largest of all Brasil flux central Amazon locations. By contrast, models simulated a peak in NPP_{wood} at CAX and K67 that corresponded to the beginning of the dry season. The seasonality of model NPP_{wood} was absent at the three equatorial forests, and only significant differences between the wet and dry periods were reported at RJA, where all simulations showed minimum NPP_{wood} at the end of the dry season.

Our analysis shows a statistically significant negative linear regression between SW_{down} and NPP_{wood} with a coefficient of determination, R^2 equal to 0.58 at K67 and 0.63 at CAX ($P < 0.01$) (Fig. S3). Nonsignificant correlation was found between SW_{down} and NPP_{wood} or precipitation and NPP_{wood} at K34 – the wettest and least seasonal of the four studied forests.

Seasonal observations of the different NPP components and GPP showed a lack of temporal synchrony between them. Nor was a shared allocation pattern among forests, each exhibited different phenologies (Fig. 5). At some sites (CAX and K67), there was a statistically significant correlation (~1 to 2-month lag, NPP_{leaf} ahead) between GPP and NPP_{leaf} (Fig. S5). However, there was no temporal correspondence between GPP and NPP_{wood}. By comparison, model allocation (NPP_{leaf}, $NPP_{litter\text{-}fall}$, and NPP_{wood}) and GPP were coupled at most models (Fig. 5).

Ecosystem respiration (R_e) and net ecosystem exchange (NEE)

Similar to GPP, the timing and amplitude of ecosystem respiration (R_e) seasonality at RJA was well captured by most DGVMs (Fig. S7); however, at equatorial Amazon sites all simulations overestimated R_e (Fig. 3). In particular, during the months for which R_e reached a minimum, the wet season at CAX and the dry season at K67, model R_e showed opposite seasonality to observations. The imbalance between predicted R_e and GPP translated into an underestimation of the observed net ecosystem uptake (negative NEE), with the models predicting a positive NEE (strong carbon source), in particular, at K34 and CAX. More importantly, the seasonality of NEE in the equatorial forests (K34, K67, and CAX) was missed, with the DGVMs foreseeing a greater carbon loss during the dry season, as opposed to those observed during the September–December period (Fig. 3).

Discussion

In this study, we found that dynamic global vegetation models poorly represented the annual cycle of carbon flux dynamics for the Amazon evergreen tropical forest sites with eddy covariance towers. In particular, at equatorial Amazonia, observations showed an increase in GPP, Pc, and/or LAI during the dry season. In contrast, DGVMs simulated constant or declining GPP and Pc, and in general, assumed no seasonal cycling in LAI. The disparity between model and *in situ* measurements of GPP indicated that there is a bias in the modeled ecosystem response to climate and a lack of understanding of which drivers, meteorological (e.g., light or water) or phenological (e.g., leaf demography) or a combination thereof, control ecosystem carbon flux. Moreover, a mismatch between seasonal observations of carbon pools and allocation strategies (NPP_{leaf}, NPP_{wood}, $NPP_{litter\text{-}fall}$) and model results highlights the importance of phenology as an essential tool for understanding productivity within the tropical forest of the Amazon (see Delpierre *et al*.(2015) for an in-depth description of model allocation schemes).

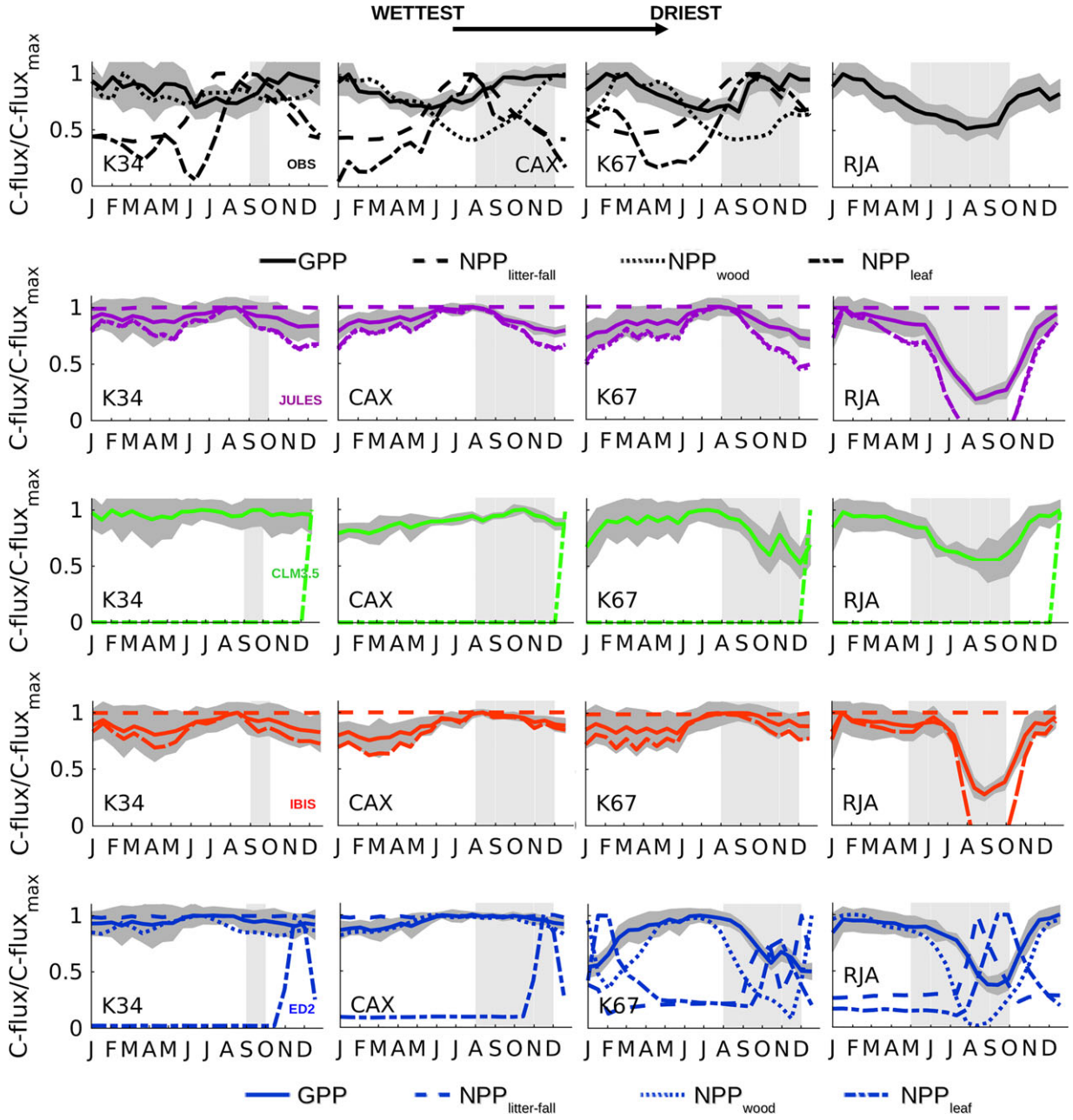

Fig. 5 From top to bottom, annual cycle observed (black) and model simulations from JULES (purple), CLM3.5 (green), IBIS (red), and ED2 (blue). Normalized (by its seasonal maximum) annual cycle of daily average ecosystem-scale photosynthesis (GPP/GPP$_{max}$) (continuous line), net primary productivity (NPP) allocated to leaves –leaf-flush (NPP$_{leaf}$ /NPP$_{leaf\ max}$), NPP allocated to litter-fall (NPP$_{litter\text{-}fall}$ /NPP$_{litter\text{-}fall\ max}$), and NPP allocated to wood (NPP$_{wood}$ /NPP$_{wood\ max}$). From left to right study sites (from wettest to driest) near Manaus (K34), Caxiuanã (CAX), Santarém (K67), and Reserva Jarú southern (RJA) forests. Gray-shaded area is dry season as defined using satellite-derived measures of precipitation (TRMM: 1998–2014).

Seasonality of gross primary productivity (GPP) and other carbon fluxes

We observed the greatest discrepancies between measured and model predicted GPP, R_e, and NEE at central Amazon sites, where productivity is hypothesized to be primarily controlled by a combination of light availability and phenology (Restrepo-Coupe *et al.*, 2013; Wu *et al.*, 2016). By contrast, models were able to capture the 'correct' seasonality at the southern forest of RJA, a site that shows significant signs of water limitation. However, at RJA the amplitude of the annual cycle

were overestimated by most DGVMs, which assume lower than expected GPP during the dry season. Our results suggest that, while models have improved their ability to simulate water stress, their ability to simulate light-based growth strategies is still an issue.

Satellite phenology studies have shown annual precipitation values and the length of the dry season to be important factors when determining ecosystem response (Guan *et al.*, 2015). Nevertheless, K67 and RJA share similar rainfall values, with MAP of 2030 mm year^{-1}, dry-season precipitation (DSP) of 50 mm month^{-1}, and a 4- to 5-month dry period, only the minimum annual precipitation differs, having RJA *MiAP* of 14 compared to 37 mm month^{-1} measured at K67. Moreover, increasing levels of incoming light at K67 and other equatorial sites during the dry season provided an opportunity for vegetation to increase productivity under the existent precipitation regime, as rainfall delivered more than 60% of ecosystem water needs assuming a monthly ~100 mm requirement (DSP >64 mm month^{-1}). For central Amazon tropical forests, observed increases in GPP, Pc, and allocation patterns, linked to light-harvesting strategies, were concurrent with the reported maxima in incoming in solar radiation (Malhado *et al.*, 2009; Restrepo-Coupe *et al.*, 2013) or/and increasing insolation and photoperiod (e.g., leaf-flush as in Wright & van Schaik (1994) and Borchert *et al.* (2015)). Our results show that the observed NPP_{leaf} and Pc annual cycle were synchronous with canopy 'greenness' seasonality detected by remote sensing. Although controversial (Samanta *et al.*, 2010; Morton *et al.*, 2014), many satellite-derived vegetation indices analysis (Huete *et al.*, 2006; Saleska *et al.*, 2007, 2016; Guan *et al.*, 2015) show evidence of similar leaf phenology, as well as phenocam (Wu *et al.*, 2016), and ground-based studies (Chavana-Bryant *et al.*, 2016; Girardin *et al.*, 2016; Lopes *et al.*, 2016). By comparison, at RJA, there was no trade-off between light, precipitation, and atmospheric demand, as solar radiation was somewhat aseasonal (with a maximum at the beginning of the wet season) and dry-season rainfall values (*MiAP*) reached <10% of mean tropical forest ET.

Here, we reported a contrast between seasonal patterns of ET and GPP (Fig. 3), as ET patterns could be simply described (>80%) by variations in radiation and GPP patterns being a more complex function of both leaf demography and environmental drivers (Restrepo-Coupe *et al.*, 2013; Wu *et al.*, 2016). In particular at RJA, the GPP decreased significant during the dry season, yet ET was essentially invariant, indicating large seasonal variations in ecosystem water-use efficiency (WUE~ GPP/ET). These changes in WUE could be associated with seasonal variations in the leaf age distribution as shown in Wu *et al.* (2016) for K67 and K34. This hypothesis predicts that old leaves would require the same amount of water per unit intercepted radiation, but would do less photosynthesis on average. A different biophysical explanation relates to ecosystem-average stomatal conductivity (*Gs*), as *Gs* would be determined by either changes in LAI or in climate (e.g., Q_{air} and/or soil moisture) that may reach a minimum during the dry season. Decreasing *Gs* reduces GPP and transpiration (*T*), but not necessarily in proportion (Nobel, 2005). Furthermore, ET includes *T*, and surface and wet leaf evaporation (*E*), where ET = *E*+*T*. At RJA soil water may contribute to some of the ET given the shallow loamy sand profile (1.2–4.0 m deep) characteristic of the site; moreover, water table depth is unknown and may similarly play an important role (Restrepo-Coupe *et al.*, 2013; Christoffersen *et al.*, 2014). Future work should address the accuracy of ET observations (energy balance closure), the partition between *E* and *T*, leaf-level seasonal changes in WUE, and ecosystem *Gs* at *RJA* and other forests.

Carbon allocation strategies

Models include LAI in the vegetation dynamics module using a variety of strategies: (i) prescribed LAI values from remote sensing sources; (ii) dynamic calculation of daily LAI (e.g., ED2); and (iii) annual LAI fixation, wherein the DGVMs allocates any changes in leaf quantity at the end of the year, when next year's carbon balance and LAI values will be calculated (e.g., CLM3.5) (Table S3). This last approach may need to be re-evaluated given the importance of phenology as an ecosystem productivity driver. Models that dynamically calculate LAI generally rely on defining a range of values for each PFT (Clark *et al.*, 2011), where the actual index will depend mostly on the phenological status of the vegetation type – a function of temperature. Although some evergreen ecosystems do respond to temperature thresholds (e.g., positive correlation between T_{air} and LAI, and a threshold at T_{air} >0 or 'heat sum' has been identified for conifer and deciduous forests in temperate areas (Khomik *et al.*, 2010; Delpierre *et al.*, 2015)), LAI and Pc at the tropical ecosystems studied here did not exhibit a statistically significant correlation with T_{air}. Moreover, model LAI values were unreasonably 2 + units above observed values (Baldocchi *et al.*, 1988; Gower *et al.*, 1999; Asner *et al.*, 2003; Sakaguchi *et al.*, 2011). Some models assumed LAI value above six (IBIS, CLM3.5, and JULES), the theoretical limit of LAI (assuming no clumping and planar leaf angle distribution) according to Beer's law. Similar to previous findings by Christoffersen *et al.* (2014) regarding DGVMs performance when simulating water fluxes, some of the model deficiencies could be resolved

by changing the parameterization of each PFT, such as the case of maximum and minimum LAI values. However, a true improvement will only come if we increase the frequency and coverage of our measurements, and a better understanding of the carbon allocation, mechanisms that control the change in LAI, and the balance between loss due to abscission, leaf production, and other ecosystem processes.

In the observations, Pc values increased during the dry season at all central Amazon sites (Restrepo-Coupe *et al*., 2013; Saleska *et al*., 2016). Elevated Pc can be achieved through leaf-flush, as younger leaves have higher leaf carbon assimilation at saturating light (A_{max}) compared to old leaves (Sobrado, 1994; Wu *et al*., 2016), or by changes in leaf herbivory, *epiphyllous* growth, and stress, among other factors. Alternatively, Pc can be increased through a surge in canopy infrastructure (quantity of leaves) measured as leaf area index (LAI) (Doughty & Goulden, 2008). Our observations suggested a combination of these two processes or Pc mostly driven by the presence of younger leaves, as we observed a small increase in LAI at K67 during the dry season (0.7 m^2per m^2 ~10% of annual mean) and a gradual decline at CAX, respectively. In order to address the relationship between leaf demography (leaf age distribution) and carbon fluxes, we presented the seasonality of *in situ* observations of NPP_{leaf} and compared it to model estimates. We have shown that, at the equatorial Amazon estimated NPP_{leaf} was synchronous with the seasonality of SW_{down} (Figs S4 and S12). Thus, increasing light may trigger new leaf production as part of a light-based growth strategy missed by the DGVMs evaluated here (Wright & van Schaik, 1994; Restrepo-Coupe *et al*., 2013; Borchert *et al*., 2015). Some vegetation schemes have introduced a time-dynamic carbon allocation: to leaves, generic roots, coarse and fine roots, etc. However, even if models assign NPP_{leaf} varying turnover time from 243 days to a maximum of 2.7 years, the timing of leaf production seems to be missed. The counterintuitive mechanism, observed at some central Amazon forests where all or most of the leaf-demography processes (leaf-fall, leaf-flush and LAI) increase during the dry season, constitutes an important challenge for modelers and plant physiologists. An appropriate model representation and further studies are required of: (i) the leaf lifespan (Malhado *et al*., 2009), (ii) the seasonality of leaf age distribution (e.g., sun and shade leaf cohorts: young, mature, old), (iii) the effect of leaf-fall on increasing light levels at lower layers of the canopy, and (iv) the relationship between leaf age and physiology (LP Albert, N Restrepo-Coupe, MN Smith *et al*., submitted), to properly characterize Amazon basin leaf phenology and associated changes in productivity. Thus, an homogeneous age cohort where all leaves have similar ability to assimilate carbon can contribute to the model simulated aseasonal Pc and GEP seasonality driven only by water availability.

Previous studies have linked the robustness of model predictions of the terrestrial ecosystem carbon response to climate change projections to the uncertainty of the different carbon pools within the models (Ahlström *et al*., 2012). Observations show that the seasonality of allocation (e.g., $NPP_{litter\text{-}fall}$) and leaf demography (e.g., NPP_{leaf}) are closely related to the fast and slow soil carbon pools (input) and ecosystem respiration. Decomposition of $NPP_{litter\text{-}fall}$ initiates the transfer of carbon to the soil microbial and the slow and passive pools in many models and determines heterotrophic respiration. Similarly, autotrophic respiration (maintenance and growth) also will be driven by live tissue allocation (NPP_{wood}, NPP_{leaf}, and NPP_{roots}). Therefore, R_e will depend on a well-characterized phenological response of litter and woody debris, wood and leaf accumulation, and the soil carbon pools. Still, in some models and according to a set of prescribed allometric relationships for each PFT, leaves, fine roots, and stems NPP are allocated at the end of each simulated year. Thus, to improve simulation-data agreement and to generate reliable projections for ecosystem response to climate perturbations, the next generation of models must include a basic mechanistic understanding of the environmental controls on ecosystem metabolism that goes beyond correlations (e.g., NPP_{leaf} vs. SW_{down}, $NPP_{litter\text{-}fall}$ vs. *Precip*) and addresses the long time adaptation to climate and their seasonality. We highlight the need for extended EC measurements accompanied by seasonal-based biophysical inventories, as both datasets complement and inform each other.

The seasonal patterns in GPP and NPP (leaf and wood); where shown to be (i) aseasonal at K34; (ii) near-synchronous at CAX; and (iii) out-of-phase at K67. By comparison, observations at flooded forests, wetter sites than those examined here, showed reduced production of new leaves and lower photosynthetic assimilation during the inundation period, and both, NPP_{wood} and NPP_{leaf} peaks shifted into the dry season (Parolin, 2000; Dezzeo *et al*., 2003). At the dry end of the wet-to-dry continuum of tropical forests, no single pattern has been described for dry tropical sites other than $NPP_{litter\text{-}fall}$ increasing during the dry period (Lieberman, 1982; Murphy & Lugo, 1986; Singh & Kushwaha, 2006; Piepenbring *et al*., 2015). The GPP, NPP_{leaf}, and NPP_{wood} dry-season maxima at CAX may be interpreted in terms of a combination of mechanisms: (i) optimal allocation patterns (Doughty *et al*., 2014) – in sync photosynthetic activity and carbon allocation driven by dry-season light increases; and (ii) reflect

biophysical limitations (Fatichi *et al.*, 2014) – wet season conditions (e.g., low radiation and high soil moisture content), drive both leaves and wood to be produced during the dry season (leaf preceding). By comparison, the NPP_{wood} patterns observed at K67 where dry-season *MiAP* is ~50% of mean annual ET may reflect biophysical limitations on the sink tissue (e.g., cell turgor and cell division in cambial tissues) – water availability as a driver (Wagner *et al.*, 2012; Rowland *et al.*, 2013), or/and an allocation strategy that favors NPP_{leaf} to NPP_{wood}. At K67 and K34 forests, the timing of GPP vs. NPP_{wood} highlights the importance of nonstructural carbon (NSC) (Fatichi *et al.*, 2014) and difficulties faced by more mechanistic DGVMs.

Although our study focuses solely on the rainforest biome, we report how small differences in the timing and amplitude of the precipitation and radiation cycles and their relationship (light vs. water availability) resulted in different patterns in the allocation and carbon uptake seasonality among the four sites (e.g., annual cycle of photosynthetic capacity vs. leaf-flush). Scaling from site to basin, across gradients in cloudiness and precipitation and corresponding variations in their seasonality found within the greater Amazonia, will require a comprehensive investigation into climate and vegetation controls on carbon flux across a continuum of light and water-driven strategies (leaf, wood, flower, fruit, and root allocation among other plant growth strategies), thus, beyond the scope of this analysis. Additionally, the fluxes and pools discussed here represent the ecosystem responses to climatology, and thus emphasize community-dominant allocation strategies. We acknowledge the diversity of phenological responses found within sites (e.g., individual species leaf phenology and traits as reported in Chavana-Bryant *et al.* (2016) and Lopes *et al.* (2016)), including the probable presence of 'light-adapted' and/or 'water-adapted' species at all forests. Future work should also explore variations in carbon flux seasonality and the ability of DGVMs to capture forest biological controls on productivity during anomalous meteorological conditions (e.g., dry vs. wet years) and interannual variability.

Final considerations for model improvement

This study identified three main tropical forest responses to climatic drivers that if understood could reduce the model vs. observation GPP discrepancies. These are (i) light harvest adaptation schemes (Graham *et al.*, 2003); (ii) response to water availability; and (iii) allocation strategies (lags between leaf and wood) (Fig. 6). We propose thorough (i) optimization patterns and (ii) thresholds (limitation) to obtain the seasonality of the different carbon pools. For example, models could incorporate some of the recent findings: (i) leaf demography as a function of light environment as in Wu *et al.* (2016) and in Malhado *et al.* (2009), and (ii)

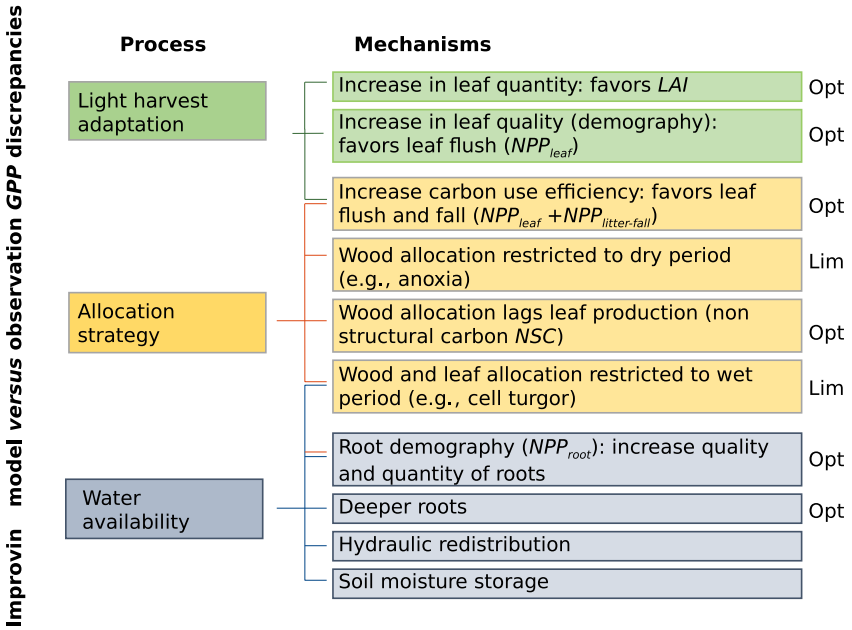

Fig. 6 Ecosystem response to climate seasonality selection of biological adaptive mechanisms: light harvest adaptations (green tones), allocation strategies (orange tones), and water limitation (blue tones). Mechanisms classified when possible into resource optimization (Opt) and biophysical limitations (Lim).

leaf phenology (greenness) seasonal patterns driven by soil moisture availability as a function of MAP threshold as in Guan *et al.* (2015). However, less has been reported about other processes and reservoirs different than NPP_{leaf} (e.g., flowering and fruit maturation). In particular, our study lacks belowground information, as data that explore the seasonality of root allocation at tropical sites is scarce and difficult to interpret (see Delpierre *et al.* (2015) for root phenology at boreal and temperate forests). Future work should address this important carbon pool and the corresponding model ability to simulate the seasonality of belowground processes.

To ensure models are obtaining the right answers for the right reasons, the robustness of a DGVM should be determined by its ability to simulate observations at timescales from hours to decades. A logical progression of model development begins with simulating observations at the timescale of greatest variation, then progressing to the greater challenge of capturing more subtle variation at other timescales (Potter *et al.*, 2001; Richardson *et al.*, 2007; Sakaguchi *et al.*, 2011). In the tropics, environmental variability is often greater within a day (amplitude of the daily cycle) than within a year (amplitude of the seasonal cycle). Thus, testing models' ability to simulate seasonality is the next step to refining DGVMs that may perform adequately at diurnal timescales. If models are able to capture seasonal carbon flux observations, it would increase our confidence that DGVMs could perform at even longer time scales (e.g., interannual variability), which is key to predict the future of tropical forests under a changing climate. Model refinement includes not only structural changes (e.g., implementation of light-adapted leaf production strategies). It also includes further study of model variability, including sensitivity tests on model parameters optimization (constrained by observations) by individual modeling groups, thus to reduce the uncertainty related to DGVM parameterization.

Climate models have come a long way, since the 1970 when the first land surface scheme was introduced in order to represent the atmosphere–biosphere interaction by partitioning ocean from dry land (Manabe & Bryan, 1969). Simulations of water, energy, and carbon fluxes based on the response of different plant functional types to climate drivers and disturbance signify a great step forward in weather prediction and the study of future climates under the effect of land cover changes and atmospheric CO_2 enrichment (Pitman, 2003; Niu & Zeng, 2012). Models are constrained in their development given the high computational needs and the multiple processes that need to be accounted for on a three dimensional grid from LAI seasonality, to ground water flux, to leaf-level parameterization, there is a trade-off and a 'priority list'. This study highlights some of the advances in tropical forest simulations of carbon and water fluxes and aims to identify future opportunities, as the inclusion of light-harvesting and allocation strategies in an attempt to improve GPP and NPP predictions.

Acknowledgements

This research was funded by the Gordon and Betty Moore Foundation 'Simulations from the Interactions between Climate, Forests, and Land Use in the Amazon Basin: Modeling and Mitigating Large Scale Savannization' project and the NASA LBA-DMIP project (# NNX09AL52G). N.R.C. acknowledges the Plant Functional Biology and Climate Change Cluster at the University of Technology Sydney, the National Aeronautics and Space Administration (NASA) LBA investigation CD-32, the National Science Foundation's Partnerships for International Research and Education (PIRE) (#OISE-0730305) and David Garces Cordoba for their funding and support. B.O.C. and J.W. were funded in part by the US DOE (BER) NGEE-Tropics project to LANL and by the Next-Generation Ecosystem Experiment (NGEE-Tropics) project from the US DOE, Office of Science, Office of Biological and Environmental Research and through contract #DESC00112704 to Brookhaven National Laboratory, respectively. The authors would like to thank Dr. Alfredo Huete, Dr. Sabina Belli, Dr. Lina Mercado, and our collaborators from the LBA-DMIP Dr. Luis Gustavo Goncalves de Goncalves and Dr. Ian Baker, and the staff of each tower site for their support, and/or technical, logistical and extensive fieldwork. We acknowledge the contributions of three anonymous reviewers whose comments helped us to improve the clarity and scientific rigor of this manuscript. Dedicated to the people of the Amazon basin.

References

Ahlström A, Schurgers G, Arneth A, Smith B (2012) Robustness and uncertainty in terrestrial ecosystem carbon response to CMIP5 climate change projections. *Environmental Research Letters*, **7**, 1–9.

Ahlström A, Raupach MR, Schurgers G *et al.* (2015) The dominant role of semi-arid ecosystems in the trend and variability of the land CO2 sink. *Science*, **348**, 895–899.

Araújo AC, Nobre AD, Kruijt B *et al.* (2002) Comparative measurements of carbon dioxide fluxes from two nearby towers in a central Amazonian rainforest: the Manaus LBA site. *Journal of Geophysical Research*, **107**, LBA 58-1–LBA 58-20.

Asner GP, Scurlock JMO, Hicke JA (2003) Global synthesis of leaf area index observations: implications for ecological and remote sensing studies. *Global Ecology and Biogeography*, **12**, 191–205.

Baker IT, Prihodko L, Denning AS, Goulden M, Miller S, da Rocha HR (2008) Seasonal drought stress in the Amazon: reconciling models and observations. *Journal of Geophysical Research*, **113**, 1–10.

Baker IT, Harper AB, da Rocha HR *et al.* (2013) Surface ecophysiological behavior across vegetation and moisture gradients in tropical South America. *Agricultural and Forest Meteorology*, **182–183**, 177–188.

Baldocchi DD, Hincks BB, Meyers TP (1988) Measuring biosphere-atmosphere exchanges of biologically related gases with micrometeorological methods. *Ecology*, **69**, 1331–1340.

Best MJ, Pryor M, Clark DB *et al.* (2011) The Joint UK Land Environment Simulator (JULES), model description – Part 1: energy and water fluxes. *Geoscientific Model Development*, **4**, 677–699.

Betts RA, Cox PM, Collins M, Harris PP, Huntingford C, Jones CD (2004) The role of ecosystem-atmosphere interactions in simulated Amazonian precipitation decrease and forest dieback under global climate warming. *Theoretical and Applied Climatology*, **78**, 157–175.

Borchert R, Calle Z, Strahler AH *et al.* (2015) Insolation and photoperiodic control of tree development near the equator. *New Phytologist*, **205**, 7–13.

Brando PM, Goetz SJ, Baccini A, Nepstad DC, Beck PSA, Christman MC (2010) Seasonal and interannual variability of climate and vegetation indices across the Amazon. *Proceedings of the National Academy of Sciences of the United States of America*, **107**, 14685–14690.

Carswell FE, Meir P, Wandelli EV *et al.* (2000) Photosynthetic capacity in a central Amazonian rain forest. *Tree Physiology*, **20**, 179–186.

Carswell FE, Costa AL, Palheta M *et al.* (2002) Seasonality in CO2 and H2O flux at an eastern Amazonian rain forest. *Journal of Geophysical Research*, **107**, LBA 43-1–LBA 43-16.

Castanho ADA, Coe MT, Costa MH, Malhi Y, Galbraith D, Quesada CA (2013) Improving simulated Amazon forest biomass and productivity by including spatial variation in biophysical parameters. *Biogeosciences*, **10**, 2255–2272.

Chambers JQ, Pereira dSR, Pereira dSE, dos SJ, Higuchi N (2013) LBA-ECO CD-08 Tree Diameter Measurements, Jacaranda Plots, Manaus, Brazil: 1999–2001.

Chambers JQ, dos Santos J, Ribeiro R, Higuchi N (2001) Tree damage, allometric relationships, and aboveground net primary production in a tropical forest. *Forest Ecology and Management*, **152**, 73–84.

Chavana-Bryant C, Malhi Y, Wu J *et al.* (2016) Leaf aging of Amazonian canopy trees as revealed by spectral and physiochemical measurements. *New Phytologist*, doi: 10.1111/nph.13853.

Chave J, Navarrete D, Almeida S *et al.* (2010) Regional and seasonal patterns of litterfall in tropical South America. *Biogeosciences*, **7**, 43–55.

Christoffersen BO, Restrepo-Coupe N, Arain MA *et al.* (2014) Mechanisms of water supply and vegetation demand govern the seasonality and magnitude of evapotranspiration in Amazonia and Cerrado. *Agricultural and Forest Meteorology*, **191**, 33–50.

Clark DB, Mercado LM, Sitch S *et al.* (2011) The Joint UK Land Environment Simulator (JULES), model description – Part 2: carbon fluxes and vegetation dynamics. *Geoscientific Model Development*, **4**, 701–722.

Collatz GJ, Ball JT, Grivet C, Berry JA (1991) Physiological and environmental regulation of stomatal conductance, photosynthesis and transpiration: a model that includes a laminar boundary layer. *Agricultural and Forest Meteorology*, **54**, 107–136.

Collatz G, Ribas-Carbo M, Berry J (1992) Coupled photosynthesis-stomatal conductance model for leaves of C4 plants. *Functional Plant Biology*, **19**, 519–538.

da Costa ACL, Galbraith D, Almeida S *et al.* (2010) Effect of 7 year of experimental drought on vegetation dynamics and biomass storage of an eastern Amazonian rainforest. *New Phytologist*, **187**, 579–591.

Cox PM, Betts RA, Bunton CB, Essery RLH, Rowntree PR, Smith J (1999) The impact of new land surface physics on the GCM simulation of climate and climate sensitivity. *Climate Dynamics*, **15**, 183–203.

Cox PM, Pearson D, Booth BB, Friedlingstein P, Huntingford C, Jones CD, Luke CM (2013) Sensitivity of tropical carbon to climate change constrained by carbon dioxide variability. *Nature*, **494**, 341–344.

De Weirdt M, Verbeeck H, Maignan F *et al.* (2012) Seasonal leaf dynamics for tropical evergreen forests in a process-based global ecosystem model. *Geoscientific Model Development*, **5**, 1091–1108.

Delbart N, Ciais P, Chave J, Viovy N, Malhi Y, Le Toan T (2010) Mortality as a key driver of the spatial distribution of aboveground biomass in Amazonian forest: results from a dynamic vegetation model. *Biogeosciences*, **7**, 3027–3039.

Delpierre N, Vitasse Y, Chuine I, Guillemot J, Bazot S, Rutishauser T, Rathgeber CBK (2015) Temperate and boreal forest tree phenology: from organ-scale processes to terrestrial ecosystem models. *Annals of Forest Science*, **73**, 5–25.

Dezzeo N, Worbes M, Ishii I, Herrera R (2003) Annual tree rings revealed by radiocarbon dating in seasonally flooded forest of the Mapire River, a tributary of the lower Orinoco River, Venezuela. *Plant Ecology*, **168**, 165–175.

Domingues TF, Berry JA, Martinelli LA, Ometto JPHB, Ehleringer JR (2005) Parameterization of canopy structure and leaf-level gas exchange for an Eastern Amazonian tropical rain Forest (Tapajós National Forest, Pará, Brazil). *Earth Interactions*, **9**, 1–23.

Doughty CE, Goulden ML (2008) Seasonal patterns of tropical forest leaf area index and CO2 exchange. *Journal of Geophysical Research*, **113**, 1–12.

Doughty CE, Malhi Y, Araujo-Murakami A *et al.* (2014) Allocation trade-offs dominate the response of tropical forest growth to seasonal and interannual drought. *Ecology*, **95**, 2192–2201.

Eltahir EAB, Bras RL (1994) Precipitation recycling in the Amazon basin. *Quarterly Journal of the Royal Meteorological Society*, **120**, 861–880.

Eva HD, Huber O (eds) (2005) A Proposal for Defining the Geographical Boundaries of Amazonia: Synthesis of the results from an Expert Consultation Workshop organized by the European Commission in collaboration with the Amazon Cooperation Treaty Organization - JRC Ispra, 7–8 June 2005.

Farquhar GD, von Caemmerer S, Berry JA (1980) A biochemical model of photosynthetic CO2 assimilation in leaves of C3 species. *Planta*, **149**, 78–90.

Fatichi S, Leuzinger S, Körner C (2014) Moving beyond photosynthesis: from carbon source to sink-driven vegetation modeling. *New Phytologist*, **201**, 1086–1095.

Fisher RA, Williams M, Costa D *et al.* (2007) The response of an Eastern Amazonian rain forest to drought stress: results and modelling analyses from a throughfall exclusion experiment. *Global Change Biology*, **13**, 2361–2378.

Foley JA, Prentice IC, Ramankutty N, Levis S, Pollard D, Sitch S, Haxeltine A (1996) An integrated biosphere model of land surface processes, terrestrial carbon balance, and vegetation dynamics. *Global Biogeochemical Cycles*, **10**, 603–628.

Friedlingstein P, Cox P, Betts R *et al.* (2006) Climate-carbon cycle feedback analysis: results from the C4MIP model intercomparison. *Journal of Climate*, **19**, 3337–3353.

Friend AD, Lucht W, Rademacher TT *et al.* (2014) Carbon residence time dominates uncertainty in terrestrial vegetation responses to future climate and atmospheric CO2. *Proceedings of the National Academy of Sciences*, **111**, 3280–3285.

Girardin CAJ, Malhi Y, Doughty CE *et al.* (2016) Seasonal trends of Amazonian rainforest phenology, net primary productivity, and carbon allocation. *Global Biogeochemical Cycles*, **30**, 2015GB005270.

de Goncalves LG, Baker I, Christoffersen B *et al.* (2009) The Large Scale Biosphere-Atmosphere Experiment in Amazônia, Model Intercomparison Project (LBA-MIP) protocol.

de Gonçalves LGG, Borak JS, Costa MH *et al.* (2013) Overview of the large-scale biosphere-atmosphere experiment in Amazonia data model intercomparison project (LBA-DMIP). *Agricultural and Forest Meteorology*, **182–183**, 111–127.

Gotangco Castillo CK, Levis S, Thornton P (2012) Evaluation of the new CNDV option of the community land model: effects of dynamic vegetation and interactive nitrogen on CLM4 means and variability*. *Journal of Climate*, **25**, 3702–3714.

Goudriaan J (1977) *Crop Micrometeorology : A Simulation Study | Wda*. Pudoc, Wageningen.

Goudriaan J (1986) A simple and fast numerical method for the computation of daily totals of crop photosynthesis. *Agricultural and Forest Meteorology*, **38**, 249–254.

Gower ST, Kucharik CJ, Norman JM (1999) Direct and indirect estimation of leaf area index, fAPAR, and net primary production of terrestrial ecosystems. *Remote Sensing of Environment*, **70**, 29–51.

Graham EA, Mulkey SS, Kitajima K, Phillips NG, Wright SJ (2003) Cloud cover limits net CO2 uptake and growth of a rainforest tree during tropical rainy seasons. *Proceedings of the National Academy of Sciences*, **100**, 572–576.

Guan K, Pan M, Li H *et al.* (2015) Photosynthetic seasonality of global tropical forests constrained by hydroclimate. *Nature Geoscience*, **8**, 284–289.

Hodnett MG, Oyama MD, Tomasella J, deMarques AOF (1996) Comparisons of long-term soil water storage behavior under pasture and forest in three areas of Amazonia. In: *Amazonia Deforestation and Climate* (eds Gash JHC, Nobre CA, Roberts JM, Victoria RL), pp. 57–77. John Wiley, New York, USA.

Huete AR, Didan K, Shimabukuro YE *et al.* (2006) Amazon rainforests green-up with sunlight in dry season. *Geophysical Research Letters*, **33**, L06405.

Huffman GJ, Bolvin DT, Nelkin EJ *et al.* (2007) The TRMM multisatellite precipitation analysis (TMPA): quasi-global, multiyear, combined-sensor precipitation estimates at fine scales. *Journal of Hydrometeorology*, **8**, 38–55.

Huntingford C, Zelazowski P, Galbraith D *et al.* (2013) Simulated resilience of tropical rainforests to CO2-induced climate change. *Nature Geoscience*, **6**, 268–273.

Hutyra LR, Munger JW, Saleska SR *et al.* (2007) Seasonal controls on the exchange of carbon and water in an Amazonian rain forest. *Journal of Geophysical Research: Biogeosciences*, **112**, 1–16.

Jacobs CMJ (1994) *Direct impact of atmospheric CO2 enrichment on regional transpiration*. Landbouwuniversiteit.

Ju W, Chen JM, Black TA, Barr AG, Liu J, Chen B (2006) Modelling multi-year coupled carbon and water fluxes in a boreal aspen forest. *Agricultural and Forest Meteorology*, **140**, 136–151.

Khomik M, Arain MA, Brodeur JJ, Peichl M, Restrepo-Coupé N, McLaren JD (2010) Relative contributions of soil, foliar, and woody tissue respiration to total ecosystem respiration in four pine forests of different ages. *Journal of Geophysical Research: Biogeosciences*, **115**, 1–17.

Kim Y, Knox RG, Longo M *et al.* (2012) Seasonal carbon dynamics and water fluxes in an Amazon rainforest. *Global Change Biology*, **18**, 1322–1334.

Kruijt B, Elbers JA, von Randow C *et al.* (2004) The robustness of eddy correlation fluxes for Amazon rain forest conditions. *Ecological Applications*, **14**, 101–113.

Kucharik CJ, Barford CC, Maayar ME, Wofsy SC, Monson RK, Baldocchi DD (2006) A multiyear evaluation of a dynamic global vegetation model at three AmeriFlux

forest sites: vegetation structure, phenology, soil temperature, and CO2 and H2O vapor exchange. *Ecological Modelling*, **196**, 1–31.

Levine NM, Zhang K, Longo M *et al.* (2016) Ecosystem heterogeneity determines the ecological resilience of the Amazon to climate change. *Proceedings of the National Academy of Sciences*, **113**, 793–797.

Lieberman D (1982) Seasonality and phenology in a dry tropical forest in Ghana. *Journal of Ecology*, **70**, 791–806.

Lopes AP, Nelson BW, Wu J *et al.* (2016) Leaf flush drives dry season green-up of the Central Amazon. *Remote Sensing of Environment*, **182**, 90–98.

Malhado ACM, Costa MH, Lima D, Z F, Portilho KC, Figueiredo DN (2009) Seasonal leaf dynamics in an Amazonian tropical forest. *Forest Ecology and Management*, **258**, 1161–1165.

Malhi Y, Pegoraro E, Nobre AD, Pereira MGP, Grace J, Culf AD, Clement R (2002) Energy and water dynamics of a central Amazonian rain forest. *Journal of Geophysical Research*, **107**, LBA 45-1–LBA 45-17.

Manabe S, Bryan K (1969) Climate calculations with a combined ocean-atmosphere model. *Journal of the Atmospheric Sciences*, **26**, 786–789.

Medvigy D, Wofsy SC, Munger JW, Hollinger DY, Moorcroft PR (2009) Mechanistic scaling of ecosystem function and dynamics in space and time: Ecosystem Demography model version 2. *Journal of Geophysical Research: Biogeosciences*, **114**, G01002.

Melton JR, Shrestha RK, Arora VK (2015) The influence of soils on heterotrophic respiration exerts a strong control on net ecosystem productivity in seasonally dry Amazonian forests. *Biogeosciences*, **12**, 1151–1168.

Metcalfe DB, Meir P, Aragão LEOC, et al. (2007) Factors controlling spatio-temporal variation in carbon dioxide efflux from surface litter, roots, and soil organic matter at four rain forest sites in the eastern Amazon. *Journal of Geophysical Research*, **112**, 1–9.

Moorcroft PR, Hurtt GC, Pacala SW (2001) A method for scaling vegetation dynamics: the ecosystem demography model (ed). *Ecological Monographs*, **71**, 557–586.

Morton DC, Nagol J, Carabajal CC *et al.* (2014) Amazon forests maintain consistent canopy structure and greenness during the dry season. *Nature*, **506**, 221–224.

Murphy P, Lugo AE (1986) Ecology of tropical dry forest. *Annual Review of Ecology and Systematics*, **17**, 67–88.

NASA (2014) Tropical Rainfall Measuring Mission Project (TRMM), 3B43: Monthly 0.25 x 0.25 degree merged TRMM and other estimates v7. *NASA Distrib. Active Arch. Cent., Goddard Space Flight Cent. Earth Sci., Greenbelt, Md*.

Niu DG-Y, Zeng DX (2012) Earth system model, modeling the land component of. In: *Climate Change Modeling Methodology* (ed. Rasch PJ), pp. 139–168. Springer, New York.

Nobel PS (2005) 8 - Leaves and Fluxes. *Physicochemical and Environmental Plant Physiology*, 3rd edn, pp. 351–418. Academic Press, Burlington.

Oleson KW, Niu G-Y, Yang Z-L *et al.* (2008) Improvements to the community land model and their impact on the hydrological cycle. *Journal of Geophysical Research*, **113**, 1–26.

Parolin P (2000) Phenology and CO2-assimilation of trees in Central Amazonian floodplains. *Journal of Tropical Ecology*, **16**, 465–473.

Piepenbring M, Hofmann TA, Miranda E, Cáceres O, Unterseher M (2015) Leaf shedding and weather in tropical dry-seasonal forest shape the phenology of fungi – Lessons from two years of monthly surveys in southwestern Panama. *Fungal Ecology*, **18**, 83–92.

Pitman AJ (2003) The evolution of, and revolution in, land surface schemes designed for climate models. *International Journal of Climatology*, **23**, 479–510.

Potter C, Klooster S, de Carvalho CR *et al.* (2001) Modeling seasonal and interannual variability in ecosystem carbon cycling for the Brazilian Amazon region. *Journal of Geophysical Research: Atmospheres*, **106**, 10423–10446.

Powell TL, Galbraith DR, Christoffersen BO *et al.* (2013) Confronting model predictions of carbon fluxes with measurements of Amazon forests subjected to experimental drought. *New Phytologist*, **200**, 350–365.

Rammig A, Jupp T, Thonicke K *et al.* (2010) Estimating the risk of Amazonian forest dieback. *New Phytologist*, **187**, 694–706.

von Randow C, Manzi AO, Kruijt B *et al.* (2004) Comparative measurements and seasonal variations in energy and carbon exchange over forest and pasture in South West Amazonia. *Theoretical and Applied Climatology*, **78**, 5–26.

von Randow C, Zeri M, Restrepo-Coupe N *et al.* (2013) Inter-annual variability of carbon and water fluxes in Amazonian forest, Cerrado and pasture sites, as simulated by terrestrial biosphere models. *Agricultural and Forest Meteorology*, **182–183**, 145–155.

Restrepo-Coupe N, da Rocha HR, da Araujo AC *et al.* (2013) What drives the seasonality of photosynthesis across the Amazon basin? A cross-site analysis of eddy flux tower measurements from the Brasil flux network. *Agricultural and Forest Meteorology*, **182–183**, 128–144.

Rice AH, Pyle EH, Saleska SR *et al.* (2004) Carbon balance and vegetation dynamics in an old-growth Amazonian forest. *Ecological Applications*, **14**, S55–S71.

Richardson AD, Hollinger DY, Aber JD, Ollinger SV, Braswell BH (2007) Environmental variation is directly responsible for short- but not long-term variation in forest-atmosphere carbon exchange. *Global Change Biology*, **13**, 788–803.

Richardson AD, Carbone MS, Huggett BA *et al.* (2015) Distribution and mixing of old and new nonstructural carbon in two temperate trees. *New Phytologist*, **206**, 590–597.

da Rocha HR, Goulden ML, Miller SD, Menton MC, Pinto LDVO, de Freitas HC, de Silva Figueira AM (2004) Seasonality of water and heat fluxes over a tropical forest in Eastern Amazonia. *Ecological Applications*, **14**, 22–32.

da Rocha HR, Manzi AO, Cabral OM *et al.* (2009) Patterns of water and heat flux across a biome gradient from tropical forest to savanna in Brazil. *Journal of Geophysical Research: Biogeosciences*, **114**, G00B12.

Rosolem R, Shuttleworth WJ, Gonçalves Ld (2008) Is the data collection period of the large-scale biosphere-atmosphere experiment in amazonia representative of long-term climatology? *Journal of Geophysical Research*, **113**, 12.

Rowland L, Malhi Y, Silva-Espejo JE *et al.* (2013) The sensitivity of wood production to seasonal and interannual variations in climate in a lowland Amazonian rainforest. *Oecologia*, **174**, 295–306.

Sakaguchi K, Zeng X, Christoffersen BJ, Restrepo-Coupe N, Saleska SR, Brando PM (2011) Natural and drought scenarios in an east central Amazon forest: fidelity of the Community Land Model 3.5 with three biogeochemical models. *Journal of Geophysical Research*, **116**, 1–24.

Saleska SR, Miller SD, Matross DM (2003) Carbon in Amazon forests: unexpected seasonal fluxes and disturbance-induced losses. *Science*, **302**, 1554–1557.

Saleska SR, Didan K, Huete AR, da Rocha HR (2007) Amazon forests green-up during 2005 drought. *Science*, **318**, 612.

Saleska SR, Wu J, Guan K, Araujo AC, Huete A, Nobre AD, Restrepo-Coupe N (2016) Dry-season greening of Amazon forests. *Nature*, **531**, E4–E5.

Samanta A, Ganguly S, Hashimoto H *et al.* (2010) Amazon forests did not green-up during the 2005 drought. *Geophysical Research Letters*, **37**, L05401.

Sellers PJ (1985) Canopy reflectance, photosynthesis and transpiration. *International Journal of Remote Sensing*, **6**, 1335–1372.

Shao P, Zeng X, Sakaguchi K, Monson RK, Zeng X (2013) Terrestrial carbon cycle: climate relations in eight CMIP5 earth system models. *Journal of Climate*, **26**, 8744–8764.

Shuttleworth WJ (1988) Evaporation from Amazonian rainforest. *Proceedings of the Royal Society of London. Series B, Biological Sciences*, **233**, 321–346.

Singh KP, Kushwaha CP (2006) Diversity of flowering and fruiting phenology of trees in a tropical deciduous forest in India. *Annals of Botany*, **97**, 265–276.

Sitch S, Smith B, Prentice IC *et al.* (2003) Evaluation of ecosystem dynamics, plant geography and terrestrial carbon cycling in the LPJ dynamic global vegetation model. *Global Change Biology*, **9**, 161–185.

Sobrado MA (1994) Leaf age effects on photosynthetic rate, transpiration rate and nitrogen content in a tropical dry forest. *Physiologia Plantarum*, **90**, 210–215.

Sombroek W (2001) Spatial and temporal patterns of Amazon rainfall. Consequences for the planning of agricultural occupation and the protection of primary forests. *Ambio*, **30**, 388–396.

Stockli R (2007) LBA-MIP driver data gap filling algorithms.

Stoy PC, Katul GG, Siqueira MBS, Juang J-Y, Novick KA, Uebelherr JM, Oren R (2006) An evaluation of models for partitioning eddy covariance-measured net ecosystem exchange into photosynthesis and respiration. *Agricultural and Forest Meteorology*, **141**, 2–18.

Taylor KE (2001) Summarizing multiple aspects of model performance in a single diagram. *Journal of Geophysical Research*, **106**, 7183–7192.

Wagner F, Rossi V, Stahl C, Bonal D, Hérault B (2012) Water availability is the main climate driver of neotropical tree growth. *PLoS ONE*, **7**, e34074.

Wang W, Ciais P, Nemani RR *et al.* (2013) Variations in atmospheric CO2 growth rates coupled with tropical temperature. *Proceedings of the National Academy of Sciences of the United States of America*, **110**, 13061–13066.

Wang X, Piao S, Ciais P *et al.* (2014) A two-fold increase of carbon cycle sensitivity to tropical temperature variations. *Nature*, **506**, 212–215.

Werth D, Avissar R (2002) The local and global effects of Amazon deforestation. *Journal of Geophysical Research*, **107**, LBA 55-1–LBA 55-8.

Wright SJ, van Schaik CP (1994) Light and the phenology of tropical trees. *American Naturalist*, **143**, 192–199.

Wu J, Albert LP, Lopes AP *et al.* (2016) Leaf development and demography explain photosynthetic seasonality in Amazon evergreen forests. *Science*, **351**, 972–976.

Würth MKR, Peláez-Riedl S, Wright SJ, Körner C (2005) Non-structural carbohydrate pools in a tropical forest. *Oecologia*, **143**, 11–24.

Supporting Information

Additional Supporting Information may be found in the online version of this article:

Figure S1 Locations of eddy covariance tower study sites at the Amazon Basin *sensu-stricto* (Eva and Huber (eds), 2005).
Figure S2 Type II linear regression between 16-day time series of net primary productivity allocated to litter–fall ($NPP_{litter\text{-}fall}$; gC m^{-2} day^{-1}) and incoming solar radiation (SW_{down}) at upper panels.
Figure S3 Type II linear regression between 16-day time series for each site: lagged (1.5 month) and non-lagged net primary productivity allocated to wood (NPP_{wood}; gC m^{-2} day^{-1}) and precipitation (*PrecipTRMM*; mm $month^{-1}$) at upper panels.
Figure S4 Type II linear regression between 16-day time series of net primary productivity allocated to leaves (NPP_{leaf}; gC m^{-2} day^{-1}) and incoming solar radiation (SW_{down}; W m^{-2}) at upper panels.
Figure S5. Type II linear regression between 16-day time series of gross ecosystem productivity (GPP; gC m^{-2} day^{-1}) and net primary productivity allocated to leaves (NPP_{leaf}; gC m^{-2} day^{-1}), and GPP and NPP allocated to litter-fall ($NPP_{litter\text{-}fall}$; gC m^{-2} day^{-1}) at upper panels.
Figure S6 Type II linear regression between 16-day time series of leaf area index (LAI; m^2 m^{-2}) and air temperature (T_{air}; °C) at the top row.
Figure S7 Taylor diagrams for a statistical summary of model (color coded) fluxes compared to observations at Manaus forest (K34), Caxiuana forest (CAX), Santarem forest (K67), and Reserva Jaru southern forest (RJA).
Figure S8 Taylor diagrams for a statistical summary of model (color coded) fluxes compared to observations at Manaus forest (K34), Caxiuana forest (CAX), Santarem forest (K67), and Reserva Jaru southern forest (RJA).
Figure S9 Taylor diagrams for a statistical summary of model (color coded) fluxes compared to observations at Manaus forest (K34), Caxiuana forest (CAX), Santarem forest (K67), and Reserva Jaru southern forest (RJA).
Figure S10 Linear regression 16-day average Tropical Rainfall Measuring Mission (TRMM) data product from 1998–2013 (TRMM prec) and site-specific measurements of rainfall (Precip) in mm $month^{-1}$.
Figure S11 Annual cycle of monthly average precipitation (*Precipitation*; mm $month^{-1}$ from the Tropical Rainfall Measuring Mission (TRMM) (NASA, 2014) based on an annual composite for the years 1998 to 2013.
Figure S12 From left to right study sites (from wet to dry forest) near Manaus forest (K34), Caxiuana forest (CAX), Santarem forest (K67), and Reserva Jaru southern forest (RJA).
Table S1 Site specific annual day-time mean and standard deviation of photosynthetic active radiation (PAR, μmol m^{-2} s^{-1}) , vapour pressure deficit (VPD, kPa), air temperature (T_{air} ° K), and cloudiness index (CI).
Table S2 Model description: Carbon dynamics, as from LBA-DMIP.
Table S3 Model description: Vegetation dynamics, as from LBA-DMIP.